Naval Command,
Control and Ocean
Surveillance Center RDT&E Division San Diego, CA
92152-5001

Technical Document 2706
October 1994

(Previously published as TN 555, October 1978)

Marine Boundary Layer Refractive Effects in the Infrared

R. Feinberg
H. V. Hitney
H. G. Hughes

Technical Document 2706
October 1994

(Previously published as TN 555, October 1978)

Marine Boundary Layer Refractive Effects in the Infrared

R. Feinberg
H. V. Hitney
H. G. Hughes

Boundary Layer Ducting Effects on the Transmission of Infrared Wavelengths

R. Feinberg, H. V. Hitney and H. G. Hughes

Electromagnetic Propagation Division
Environmental Sciences Department
Naval Ocean Systems Center

An experiment was conducted to determine whether ducting phenomena (gradients in refractivity) occur close to the ocean surface at infrared wavelengths. A CO_2 laser beam (10.6 μm) was transmitted and received over an 8.5 km path in San Diego Bay. For the cases investigated (sea warmer than the air), the results of the study indicate that for air temperature gradients less than $1^{o}C$/meter, the distance to the infrared horizon was only 60% of the normal geometrical horizon.

TABLE OF CONTENTS

I. INTRODUCTION

Predicting the effects of changing weather conditions and atmospheric constituents on sensor performance, remains an outstanding Navy problem in the design and development of improved electro-optical (EO) systems. Of special interest here are the forward-looking infrared (flir) imaging systems whose performance is severely limited in regions of high humidity. This is the case to be expected for flir systems operated from periscopes near the ocean surface.

EO systems performance close to the ocean surface can also be affected by differences between the sea (T_s) and air (T_a) temperatures. Moderate temperature gradients can result in large gradients in the optical and infrared refractivity. This can give rise to refraction (or bending) of imaged rays which may either increase or reduce (depending upon the sign of the temperature difference) the detection ranges of flir systems.

In the standard atmosphere (where the temperature lapse rate is of the order of $0.6^{\circ}C/100$ metres) light rays are bent downward but with a radius of curvature greater than that of the earth. To an observer on the earth, the rays appear to be bent slightly upward. The standard optical horizon is therefore only about 8% greater than the geometrical horizon. When a target is located over the standard optical horizon as depicted in Figure I-1 (distances not drawn to scale), it would be outside the field of view of a flir system operating close to the ocean surface and escape detection. When the temperature gradient ($T_s<T_a$) is of the order of $1^{\circ}C/metre$, strong bending of the rays towards the earth can occur. This is illustrated in Figure I-2 where infrared radiation emitted by a surface target is shown ducted to a detection system beyond the standard optical horizon. When $T_s>T_a$, rays are strongly bent upward, thereby shortening the optical horizon and limiting the detection range as shown in Figure I-3.

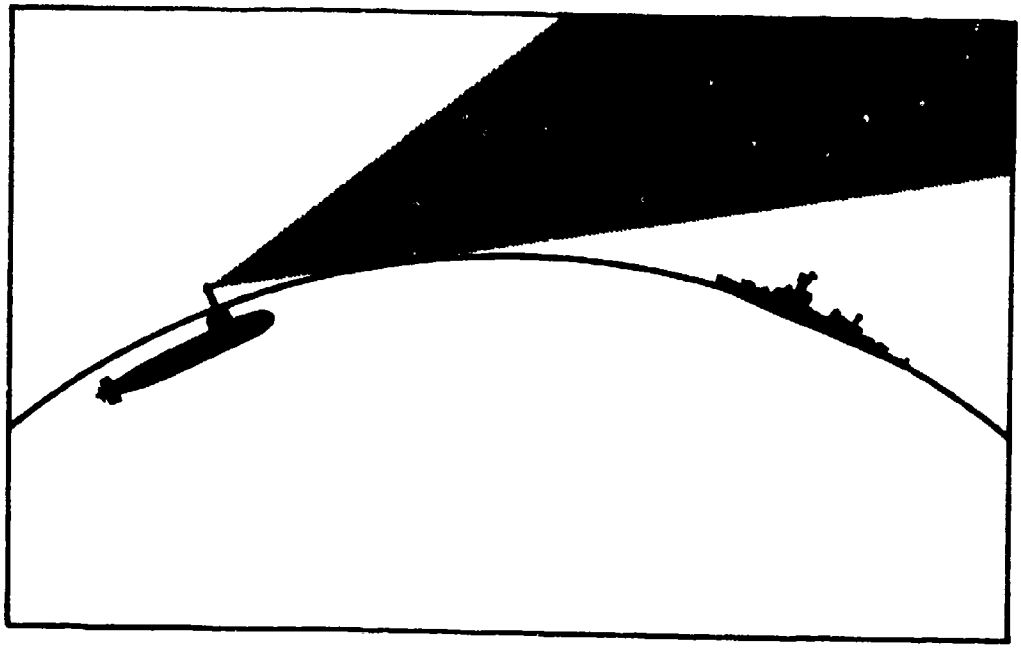

Figure I-1. Target beyond standard optical horizon.

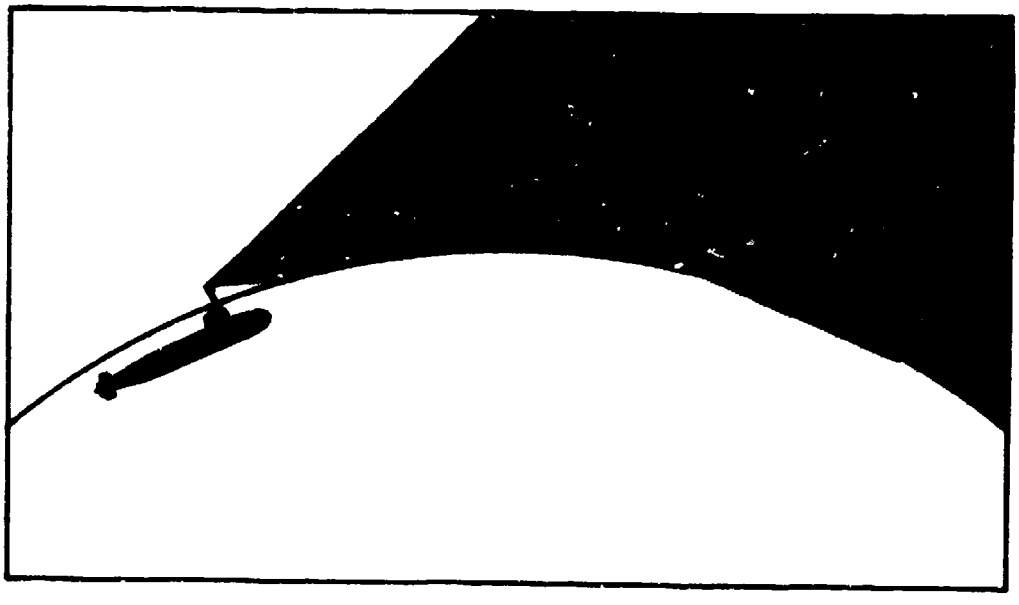

Figure I-2. Target within extended horizon ($T_{sea} < T_{air}$).

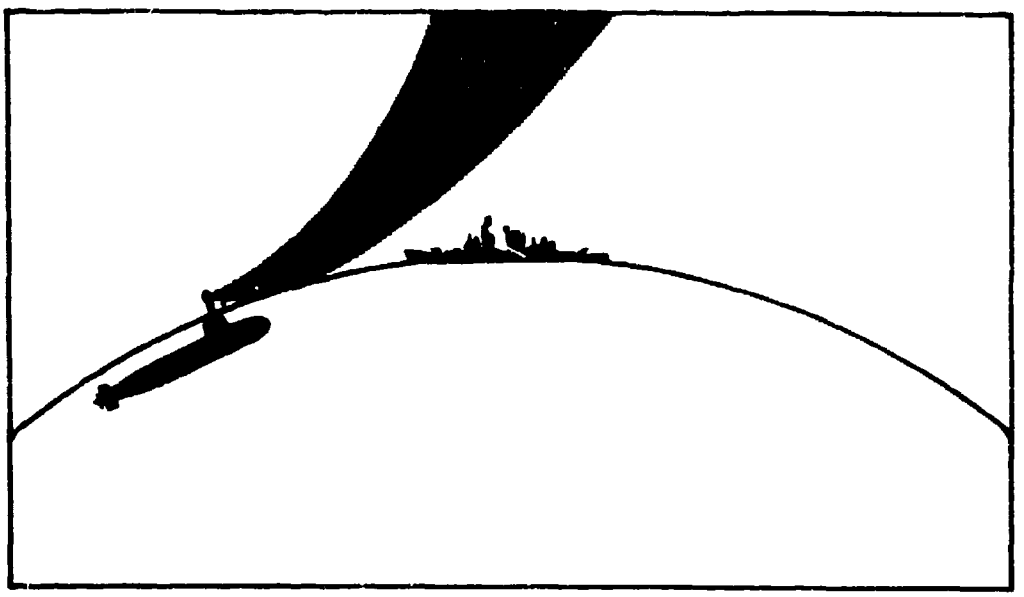

Figure I-3. Target beyond shortened horizon ($T_{sea} > T_{air}$).

There is adequate evidence of the occurrence of ducting phenomena (mirages) for visible wavelengths. Examples are shown in Figure I-4 of how objects can be distorted when viewed from different heights above the sea surface. The pictures (a), (b) and (c) show objects in San Diego Bay when viewed from heights above the water surface of approximately 1.5, .3 and .15 metres, respectively. Seen in (a) and (b) are an abandoned floating house, a "saucer" shaped house boat, and spar and ball buoys. The distance to the stilt house is approximately 4 km and the saucer boat is 3 km. At a height of 1.5 metres, inferior images of the stilt house and saucer boat are beginning to form and become more pronounced when the viewing height is lowered to .3 metre. Note also the position of the spar buoy and its image relative to the stilt house in (a) and (b), and also the inverted image of the ball buoy. When viewed from a height of .15 metres, in (c), an apparition of the saucer boat looms above the horizon as a two-image inferior mirage indicating the presence of a strong positive gradient in optical refractivity (ducting) close to the water surface. If similar ducting conditions exist for IR wavelengths, the detection ranges of flir systems may be enhanced. However, the resulting mirage effects may also degrade the system's target identification capabilities. It also must be determined whether the effects of water vapor absorption, wind, and sea surface roughness counteract the ducting conditions.

Reported in this technical note are the results of an investigation to determine if ducting influences the long range propagation of IR wavelengths close to the ocean surface. Presented in the following sections are the analytical background of refraction and computer programs which were developed to model the refractive effects; the experimental approach; the instrumentation description; measurements and data analyses; and conclusions. The work was accomplished under NOSC IR/IED funding, problem number ZR625and covers the period from 1 October 1977 to 30 September 1978.

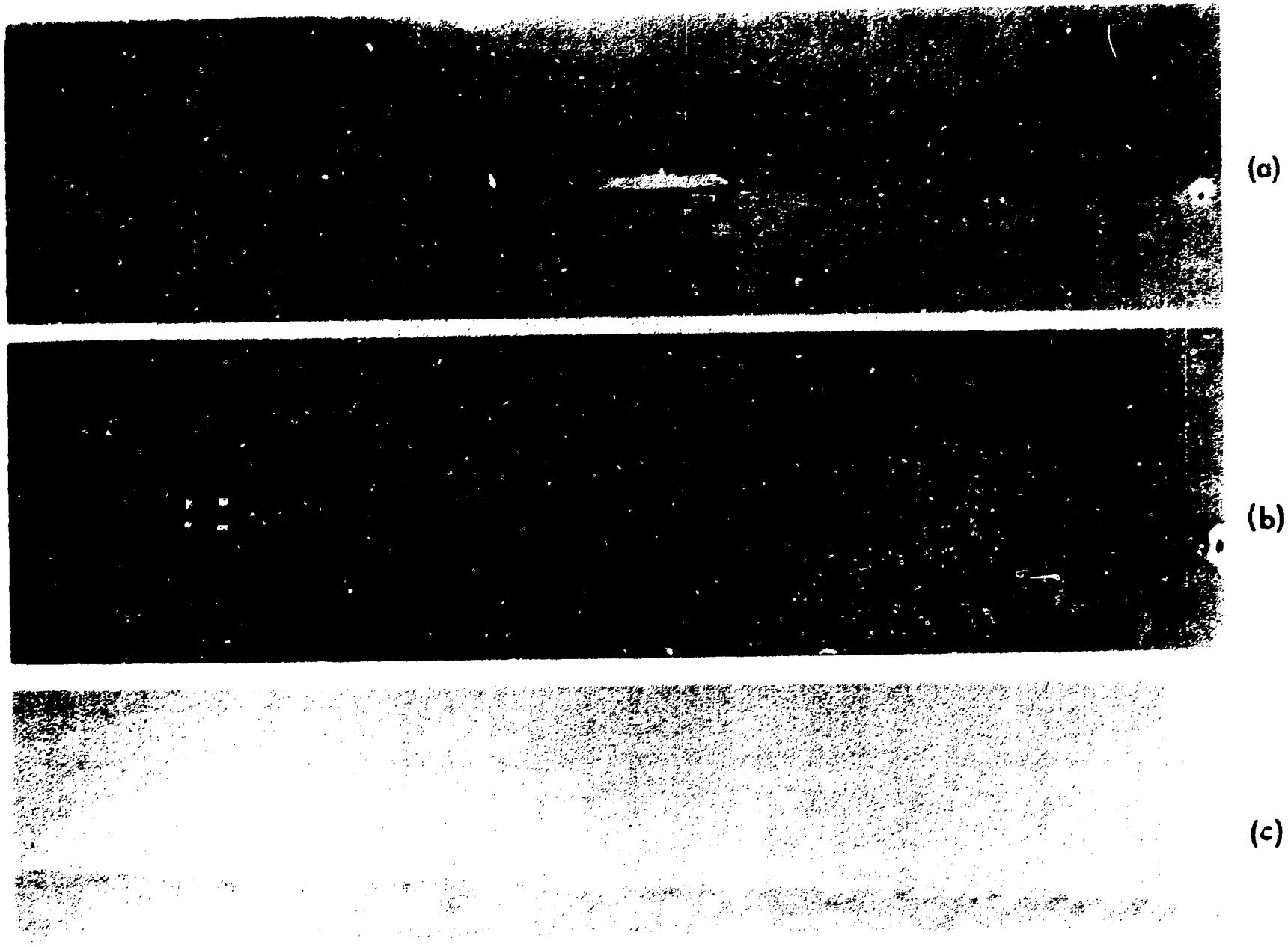

Figure I-4. Various objects viewed near the sea surface. Observer height is 1.5 m in (a), 0.3 m in (b), and 0.15 m in (c).

II. BACKGROUND

A. Atmospheric Attenuation

The atmosphere attenuates light waves by two mechanisms, scattering and absorption. At visible wavelengths, extinction is primarily due to scattering by atmospheric gases and aerosols. Infrared wavelengths however, lose energy both by aerosol scattering and absorption, and by gaseous absorption. The magnitude of the contribution to total extinction by each mechanism depends upon the optical properties, atmospheric concentration and temperature of the molecular or particulate species.

In the 8-12 μm region, the dominant contribution to extinction by molecular absorption is that from water vapor. For high humidities, refractive effects which are normally observable in the visible, may not be apparent when viewed at IR wavelengths due to the high attenuation. The effects of temperature and relative humidity on the transmittance (ratio of power received to that transmitted) of a 10.6 μm wavelength source over an 8.5 km path is shown in Figure II-1. The calculations were performed using the LOWTRAN 3B (Selby, et al.) atmospheric transmission model and aerosol effects were not considered. The limitations of humidity on transmittance are readily apparent. For example, at an air temperature of 20°C and 85% relative humidity, only 10% of the transmitted power reaches the detector. Conversely, for haze conditions and low relative humidities, the scattering by aerosols may mask ducting at visible wavelengths but leave the infrared wavelengths unaffected.

B. Refractivity

Light waves travel through the atmosphere with a velocity v which is less than that for free space, c, by a factor of 1/n where n is the index of refraction. If n changes along the wavefront (normal to the direction of propa-

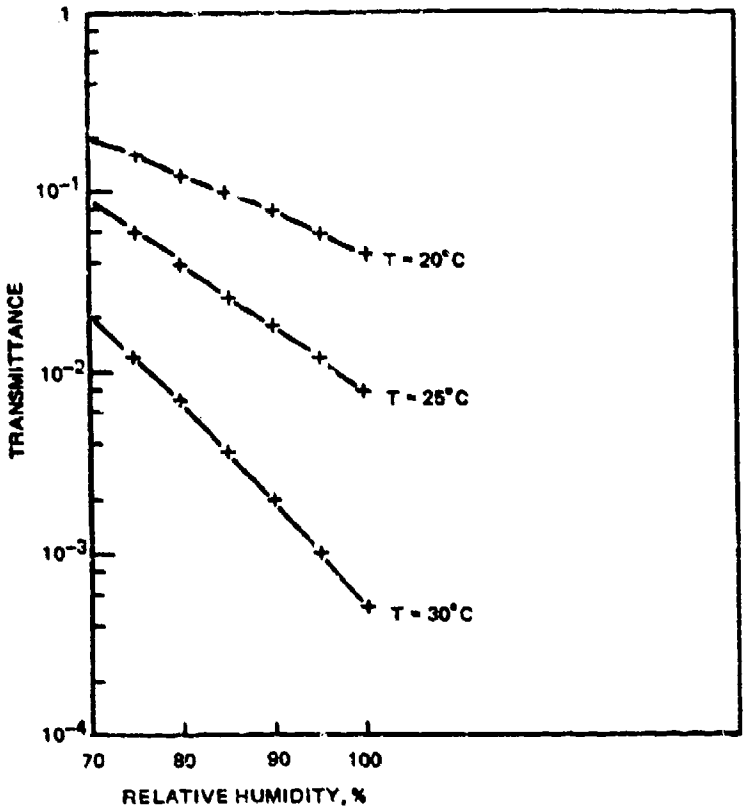

Figure II-1. Transmittance of 8.5 km path at 10.6 μm vs. relative humidity for various temperatures.

gation), different portions of the wave travel with different velocities causing bending or distortion of the wavefront. In air however, light waves are bent through such small angles, that objects appear distorted only when viewed from distances of several kilometres.

Because the index of refraction of air is close to unity (1.00032 at STP), it is convenient to define the quantity N, given by

$$N = (n-1) \cdot 10^6 \tag{1}$$

which is the refractive modulus or refractivity. For light waves, the refractivity of air depends upon the air density and not the water vapor pressure as it does for radio frequencies. For a wavelength λ, the refractivity is given by

$$N \equiv (n-1) \cdot 10^6 = 77.6 \frac{P}{T} + 0.584 \frac{P}{T\lambda^2} \tag{2}$$

where P is the barometric pressure in millibars and T is the air temperature in degrees Kelvin. While there is a slight wavelength dependency on N (3% difference between N values at .5 μm and 10 μm), it is the gradients in T and P that determine ducting, and all optical frequencies should be equally affected. The vertical gradients in T and P can be introduced into equation (2) by logarithmic differentiation with respect to the vertical ordinate, Z:

$$\frac{1}{n-1} \frac{\partial(n-1)}{\partial Z} = \frac{1}{P} \frac{\partial P}{\partial Z} - \frac{1}{T} \frac{\partial T}{\partial Z} \tag{3}$$

Replacing the index of refraction by c/v and introducing the equation of state and the hydrostatic equation into the pressure gradient term of (3) we arrive at

$$\frac{c}{v(c-v)} \frac{\partial v}{\partial Z} = \frac{Mg}{RT} + \frac{1}{T} \frac{\partial T}{\partial Z} \tag{4}$$

where M is the molecular weight of air, g is the acceleration of gravity and R is the universal gas constant.

C. Apparent Elevation for Linear Gradients

The difference between the true and apparent elevation of an object can be now estimated if we assume the temperature gradient to vary linearly with height (Fleagle, 1963). In Figure II-2, assume the temperature to decrease with altitude and the object and observer to be at the same height above a flat earth. Since the density decreases with altitude, the upper portion of a wave launched at an angle from the object will travel with a higher velocity than the lower portions. The ray (wave normal) will be bent downward with a radius of curvature, r, such that the object as seen from a distance S will appear to be at an elevated position h. If horizontal gradients in temperature are neglected, and for a fixed value of S, the time for the wave front to travel from the object to the observer is approximately independent of r, or $\theta r/v$ is a constant, and

$$\frac{1}{\theta}\frac{d\theta}{dr} + \frac{1}{r} = \frac{1}{v}\frac{dv}{dr} \tag{5}$$

For a nearly horizontal ray, h can be considered a prolongation of r in the vertical z direction such that $dv/dr \equiv dv/dz$ and

$$\cos\theta \simeq \frac{r}{r+h} \simeq 1 - \frac{S^2}{2r^2} \tag{6}$$

where $\cos\theta$ has been expanded in a Taylor series assuming $\theta << 1$ when $h << r$. Therefore,

$$\frac{1}{r} = \frac{2h}{S^2} \tag{7}$$

Combining equations (5) and (7) and since θ varies only slightly with r we have (upon substitution into equation (4);)

$$h = \left(\frac{n-1}{2n}\right)\frac{S^2}{T}\left(\frac{Mg}{R} + \frac{\partial T}{\partial Z}\right) \tag{8}$$

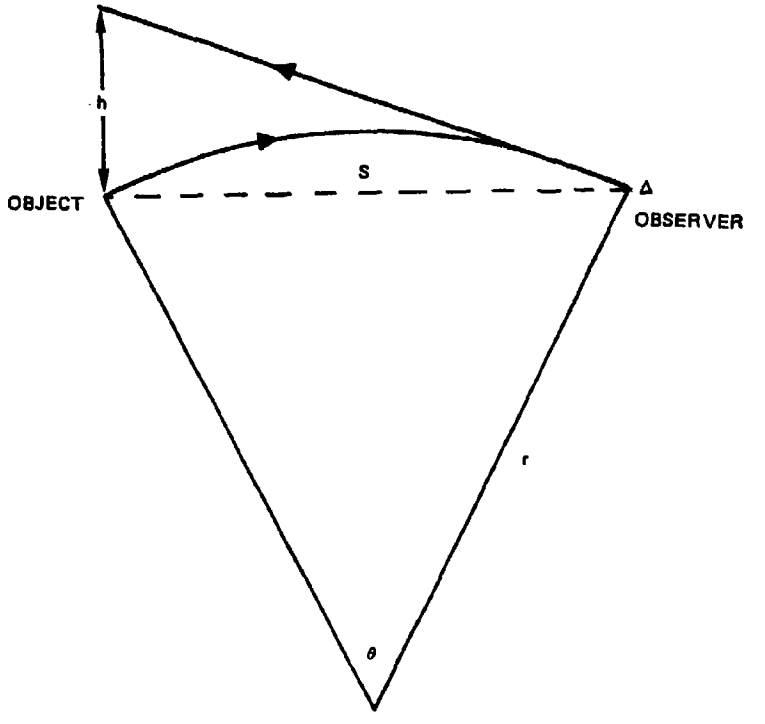

Figure II-2. Apparent position of an object when viewed by an observer at a distance S.

Equation (8) expresses the height difference with respect to a Cartesian coordinate system. To relate h to sea level the correction factor $\delta = a(\sec(s/a)-1)$ must be subtracted where a is the radius of the earth. This correction is slight for short distances but amounts to 7.8 cm at 1 km.

The apparent elevation of an object vs. temperature gradient for different distances is shown in Figure II-3. The change in elevation is less sensitive to the actual temperature than to its gradient. This is evident at a distance of 1 km where the values of h for different temperatures are compared. The figure demonstrates the effect of the sign of the temperature gradient; in general positive gradients (temperature increase with height) elevate the apparent position of the object while for negative gradients it is depressed. The effect of the pressure gradient and δ account for the fact that the lines do not pass through the origin.

D. Arbitrary Gradients

So far, we have only concerned ourselves with the effects of a linearly varying refractivity on the propagation of optical rays. However, in order to maintain complete generality, it is also necessary to consider the refractive effects resulting from an arbitrary refractivity profile.

In general, an arbitrary refractivity profile may be decomposed into any number of piecewise linear segments. Snell's law for spherical boundary surfaces (surfaces of constant index of refraction around the earth are spheres) may then be applied and the ray bending at each interface calculated. So starting with a ray of known position and inclination, it is possible to successfully raytrace its path through the atmosphere. A computer program called RAYTRACE (Appendix A) was developed to perform these calculations.

Figure II-4 shows a double image of a helium-neon laser beam propagating close to the ocean surface and viewed from a distance of 4.6 Nm. Using the

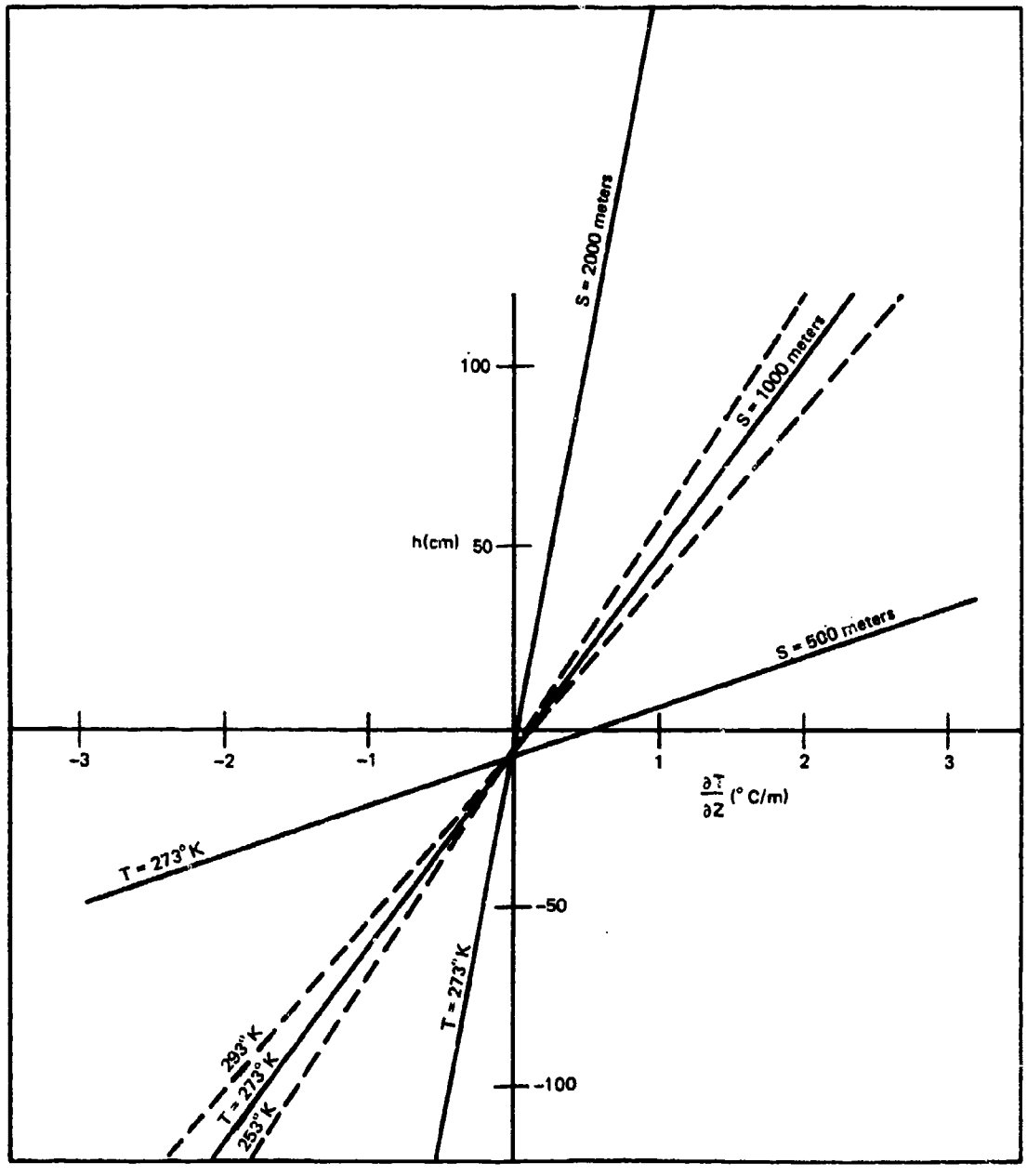

Figure II-3. Apparent elevation of an object vs. temperature gradient for various distances.

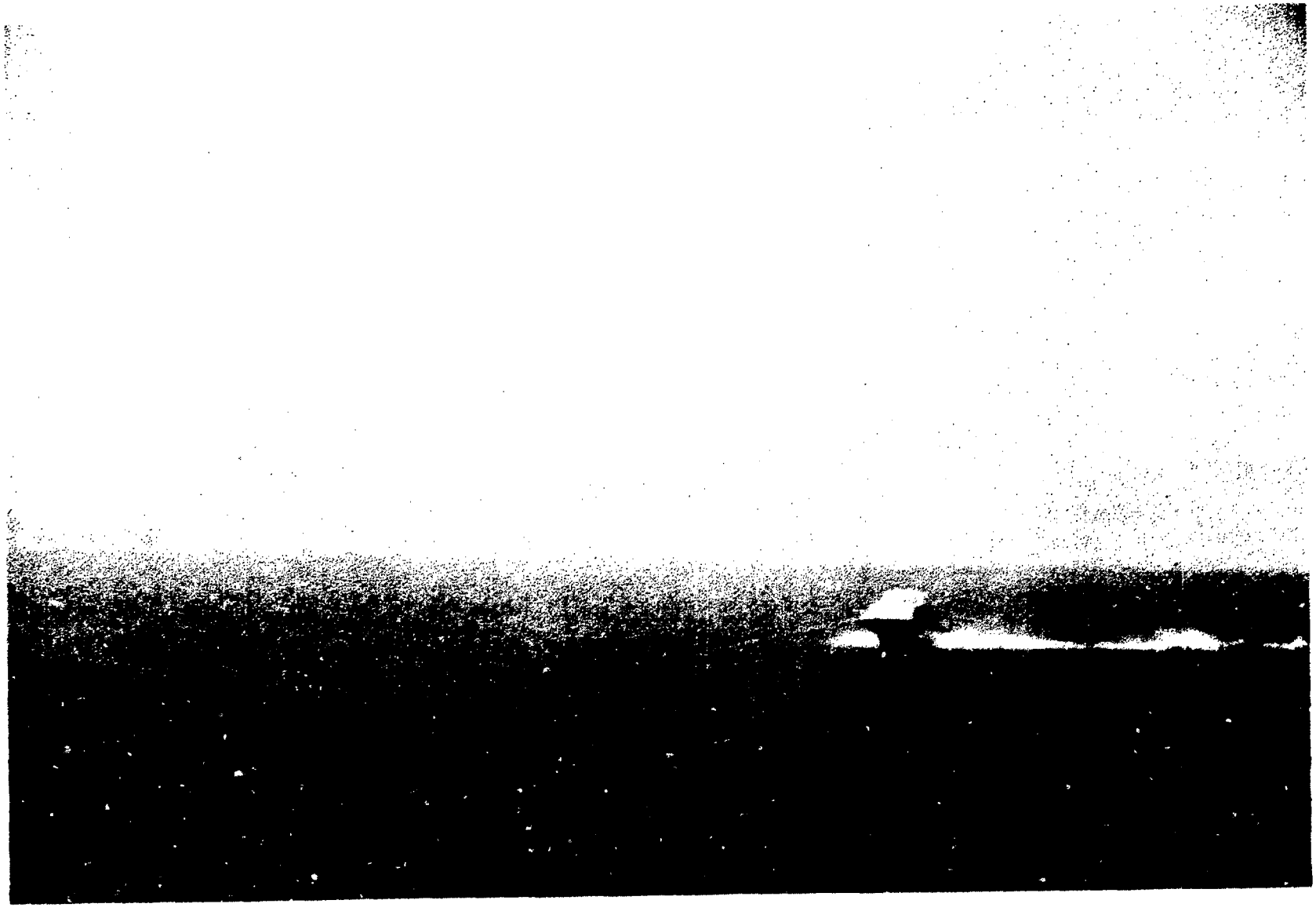

Figure II-4. Double image of He-Ne laser beam propagating close to the ocean surface.

assumed exponential temperature profile shown in Figure II-5, the computer program was able to generate the raytrace shown in Figure II-6. Notice that there are two rays which leave the source and intersect at the observing distance of 4.6 Nm. An observer at this distance located at 19 ft. above the surface, would project each ray back along the direction it reached him and form a separate image.

Examples of infrared laser beam images are shown in Figures II-7. The images were taken with a Dynard, Inc. Model 210 Fast Scan Infrared Camera which was borrowed from NOSC Code 7313. The system's detector is sensitive to the 8-14 μm wavelength band and uses a tri-metal (Hg Cd Te) detector cooled by liquid nitrogen.

Figure II-7(a) shows a double image of a CO_2 laser located 8.5 km away. The image was obtained when the tide was coming in and the detector was situated 5.25 metres above the water. The water was warmer than the air and at this point, the image shape was changing rapidly with time. In Figure II-7(b), which was taken a few minutes later, the double beam image had disappeared. These examples illustrate that image distortion can occur at IR wavelengths as well as in visible bands.

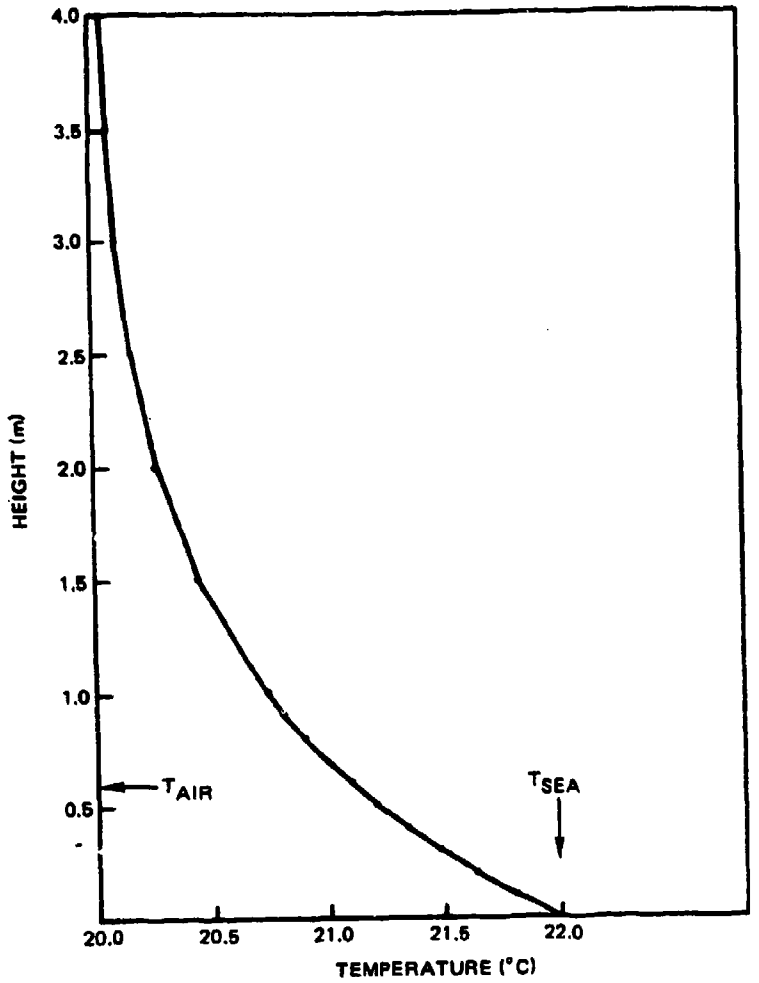

Figure II-5. Exponential temperature profile for raytrace in Figure II-6.

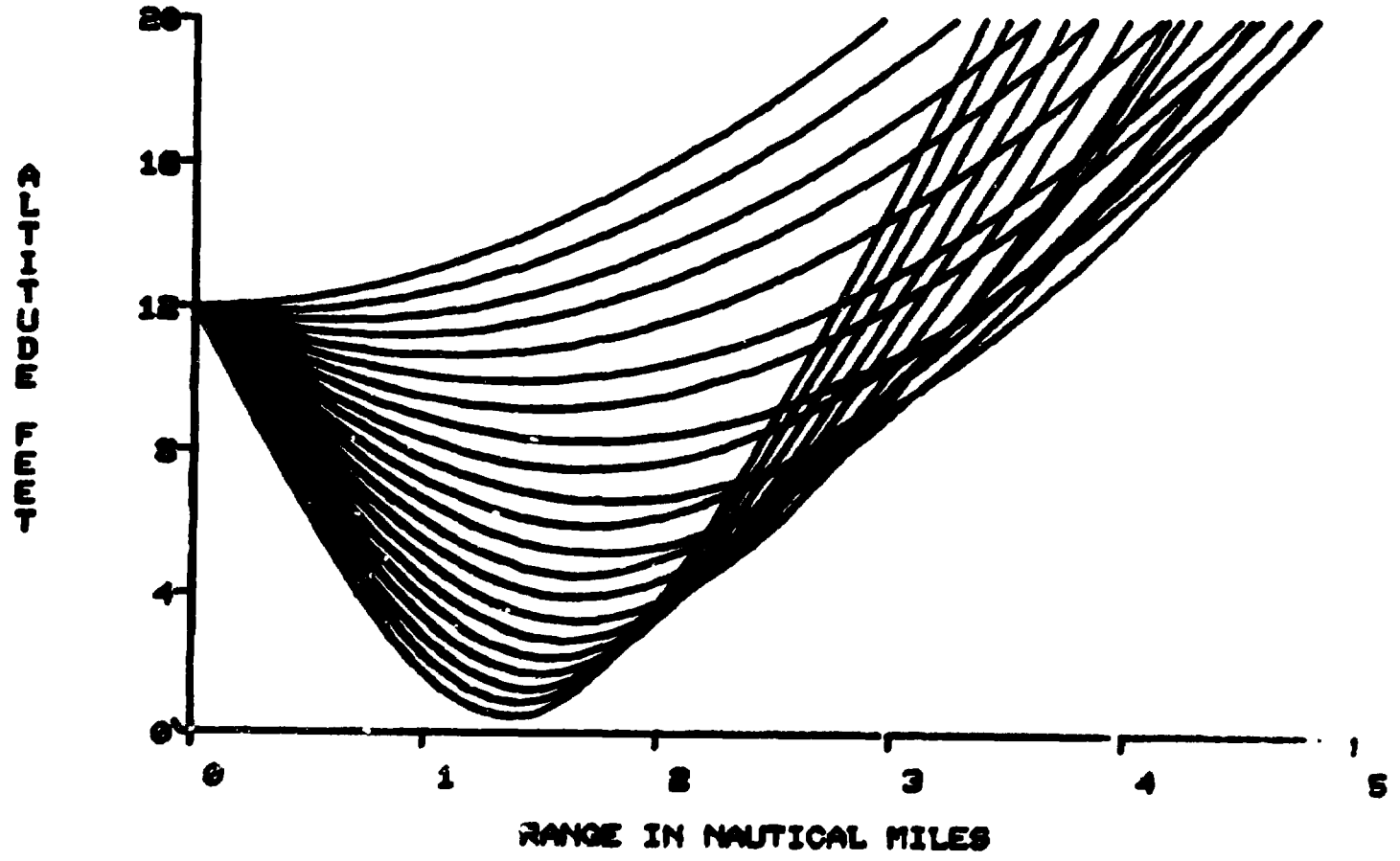

Figure II-6. Raytrace of Figure II-4 showing origin of double images.

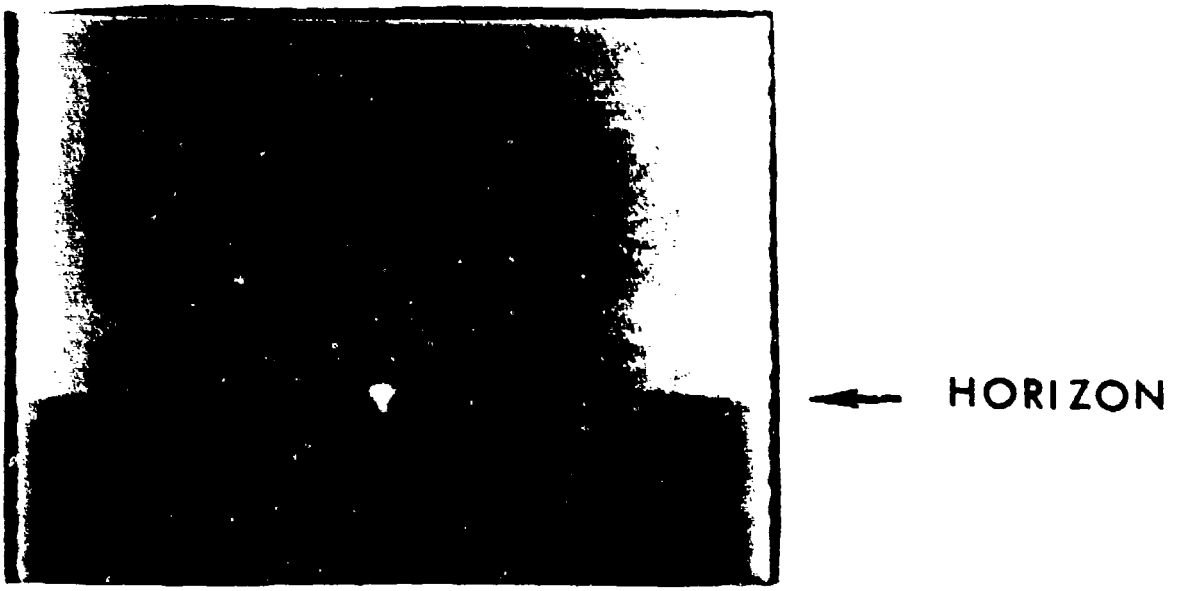

(a)

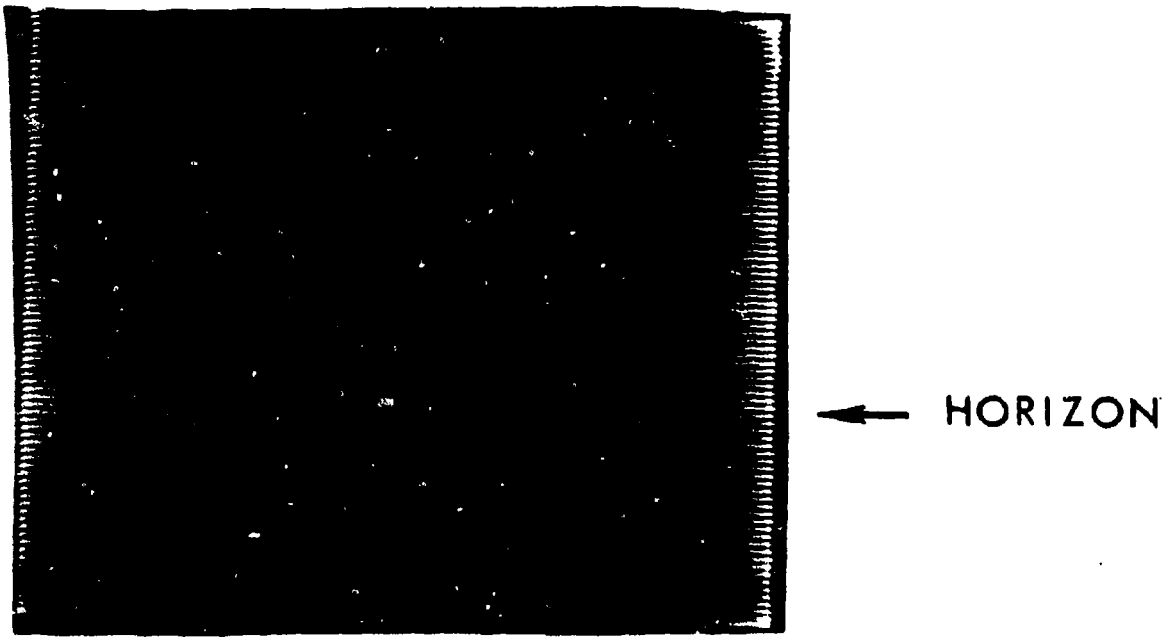

(b)

Figure II-7. Infrared images of CO_2 laser beam propagating close to the ocean surface.

III. APPROACH

The primary motivation of this research effort was in support of the DARKEYES submarine mounted flir system being developed by NOSC. The system is intended to operate close to the ocean surface. However for initial testing, it was mounted on a test stand approximately 30 metres above the ocean at NOSC building 15 on Point Loma.

A. Characterization of Image Distortions

The initial approach of the research effort was aimed at characterizing image distortions obtained by the DARKEYES system. Targets of opportunity (ships at sea and the Coronado Islands) were observed during Santa Ana periods when strong elevated optical ducting conditions were present. For this purpose, standard radiosonde transmitters were modified to respond only to temperature and pressure. The capability was developed to routinely launch the balloons from a boat at sea along the propagation path. Standard surface meteorological equipment was also installed at building 15 to measure temperature, relative humidity, pressure, visibility and aerosol size distributions.

A computer program designated IMAGE (Appendix B) was developed to model image distortion using the measured temperature profiles. Figure III-1 is a photograph of a distorted image of a ship taken from a distance of between 10 and 20 km, during a 1971 Santa Ana condition. A temperature inversion layer was present at a height of approximately 15 metres over the ocean. In Figure III-2 is shown an example of an attempt to model the distorted image using the IMAGE program and an assumed temperature gradient of .8°C/metre between altitudes of 15 and 20 metres. The temperature, T, and modified refractivity, M, profiles are shown on the left side of the figure. (The modified refractivity is given

Figure III-1. Distorted image of ship at a distance of between 10 and 20 km.

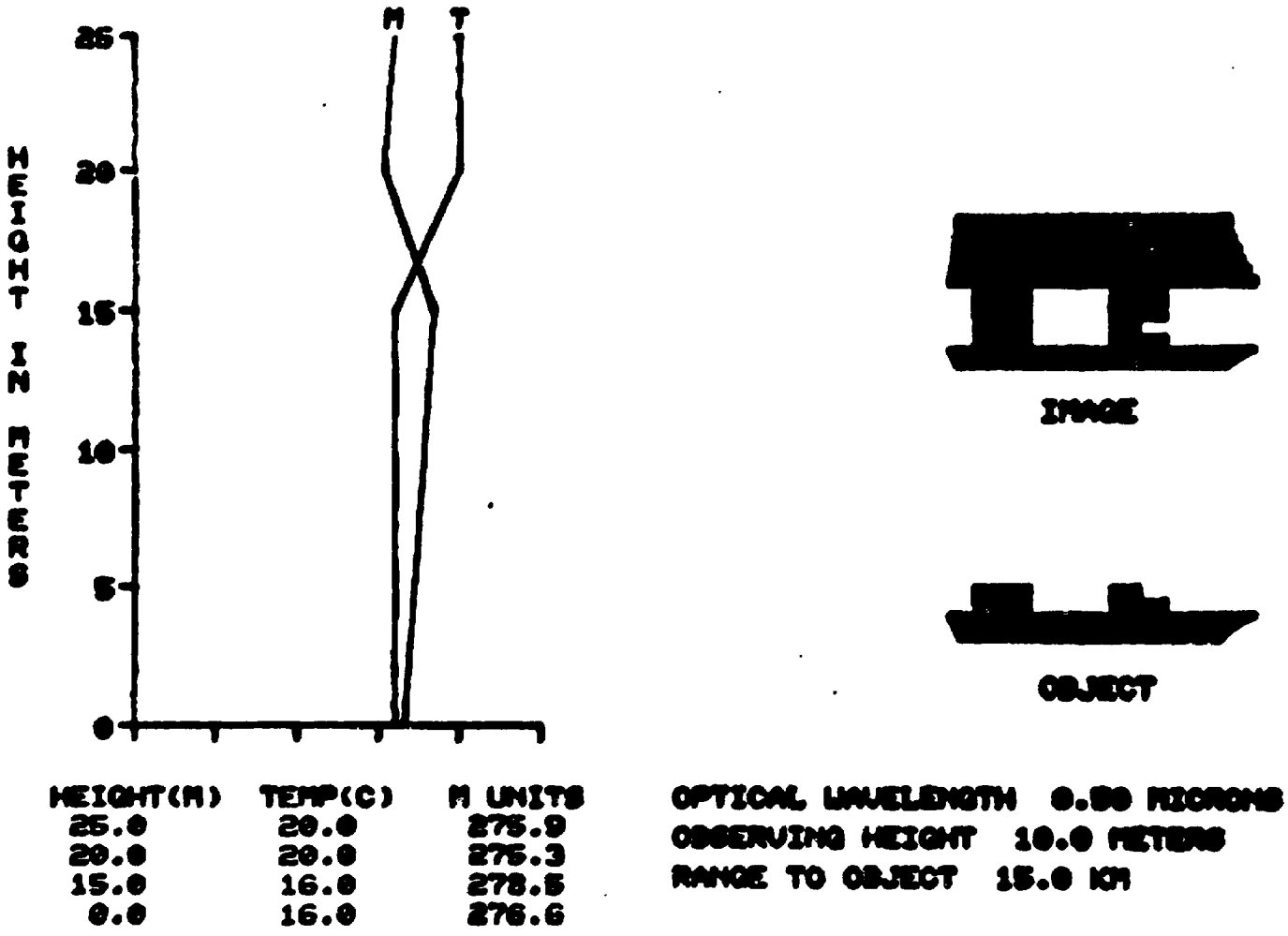

Figure III-2. Synthesized image of ship in Figure III-1 using IMAGE program.

by $M = N + (h/a)10^6$, where h is height above the surface and a is the earth's radius. M is used instead of N so that the earth can be represented by a plane in a raytrace diagram. The fictitious increase with height of refractivity provides that the difference between the curvature of the earth and the rays remains the same.)

Shown on the right side of Figure III-2 is a simulated ship configuration and its image synthesized by raytrace with the indicated refractivity profile. The height of the observer is taken to be 10 metres, the ship's height is 20 metres, and the range to the ship is 15 km. A good comparison is obtained between the synthesized ship's image and that shown in Figure III-1. The raytrace diagram used to construct the distorted image is shown in Figure III-3. From a distance of 15 km, the rays emitted from portions of the ship above about 3 metres, reaching an observer at 10 metres, appear to be coming from two different directions. This results in a two-image "superior mirage." The upper image appears inverted and elongated while the lower image is upright and slightly depressed.

This describes the method by which it was initially intended to characterize the images obtained by the DARKEYES system. However, during the period (Oct 77-Feb 78) when the system was operated, Santa Ana occurrences were rare and the temperature inversions were usually below the sensor height as illustrated in Figure III-4. For this case, only the rays from the lower portions of the object are bent by the refractivity gradient of the inversion layer. The major portions of the image are therefore undistorted.

When elevated optical ducts are present, image distortion can occur only when the object and the detector are in or near the temperature inversion layer. This is illustrated in Figure III-5 for the case when the detector and object

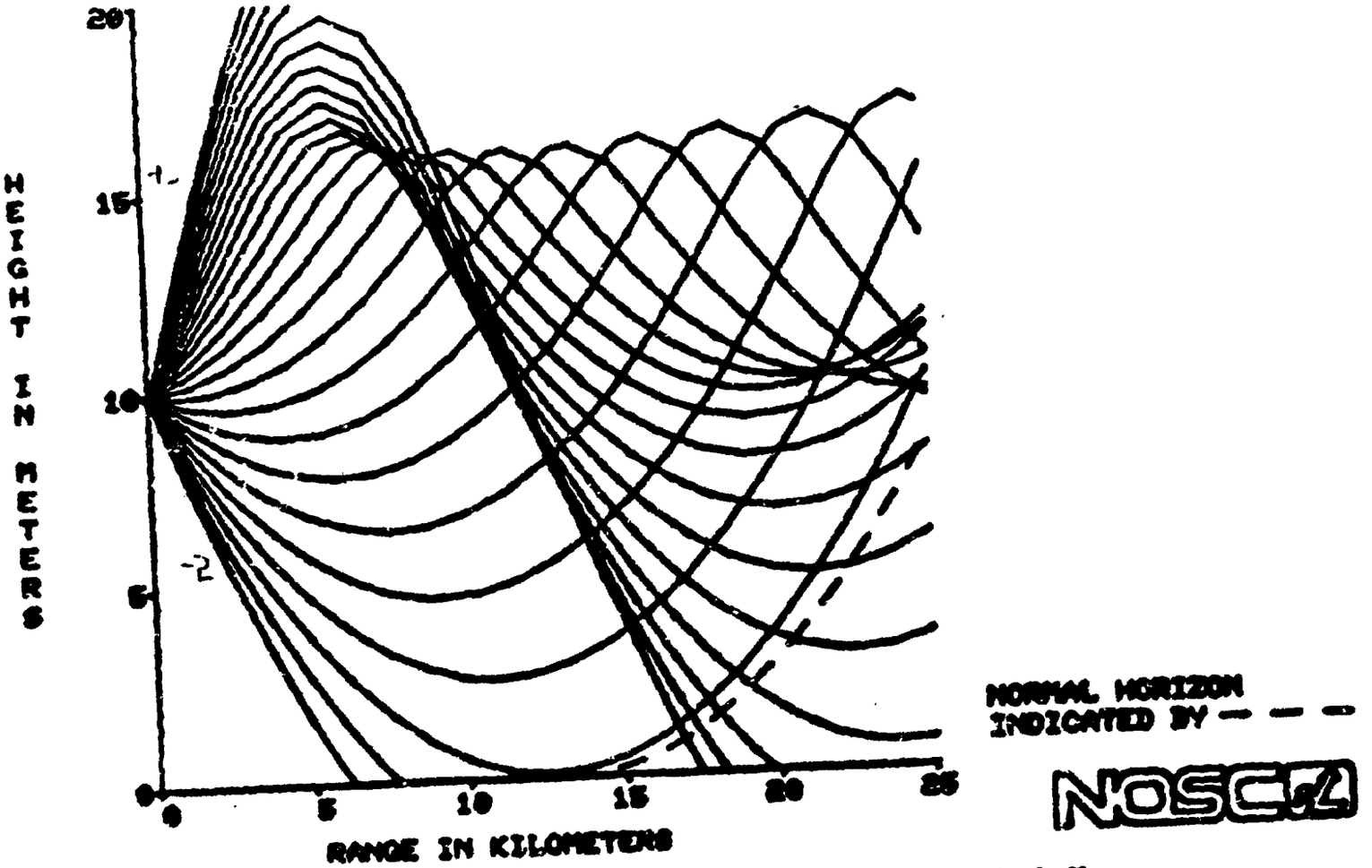

Figure III-3. Raytrace diagram used to construct image in Figure III-2.

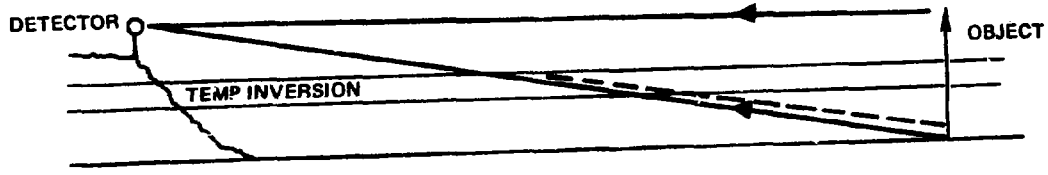

Figure III-4. Diagram of image distortion due to temperature inversion below detector.

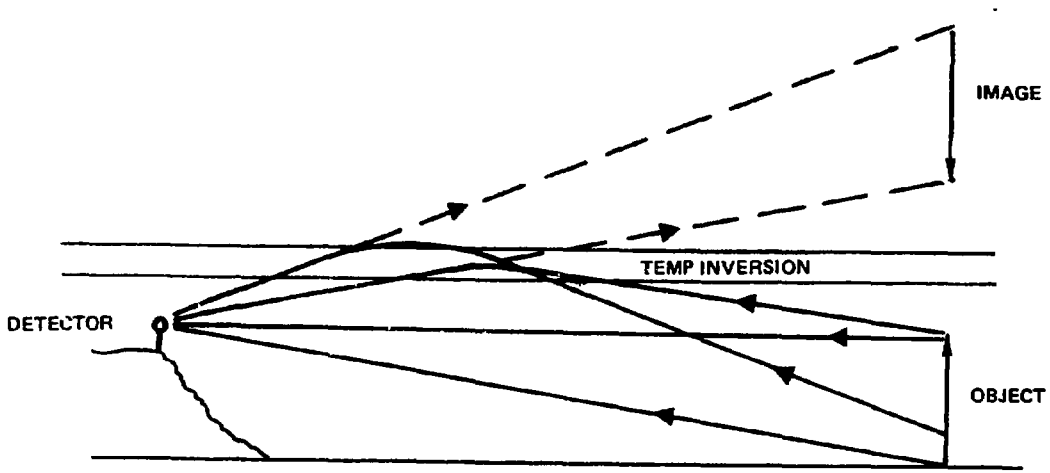

Figure III-5. Diagram of image distortion due to temperature inversion above detector.

are both slightly below the temperature inversion layer. Rays from the object are bent downward by the refractivity gradient and a second image appears at the detector inverted and at an elevated position.

During only one mild Santa Ana event (2 December 1977) was an inversion layer observed near the required 30 metres height. Figure III-6 is a photograph taken during this period showing a visually distorted image. The photograph was taken from a location approximately 3 km north of the DARKEYES facility and from the same height. The ship, determined to be an LST at an unknown distance, was not detected by the DARKEYES system. However, this may have been because the ship was at too large a distance to have been within the detection sensitivity of the system.

At the end of February 1978, the DARKEYES system was taken to sea aboard a submarine for TECHEVAL, and considerable time was spent in attempting to obtain an alternative thermal imaging system which could be operated close to the ocean surface. Several commercially available thermal imaging systems which use pyroelectric vidicon detectors were evaluated. However, those with cost within the budget limitations of the project were determined not to have sufficient resolution and sensitivity to resolve distant targets.

B. Laser Transmission Link

As an alternative means of investigating ducting phenomena at IR wavelengths close to the ocean surface, the following approach was adopted. An infrared laser and detector were positioned such that a line of sight path existed between them at low tide (Figure III-7). Here it is assumed that at low tide, the beam path is sufficiently elevated from the ocean surface so that at no time it passes through regions of strong refractivity. This is probably a good assump-

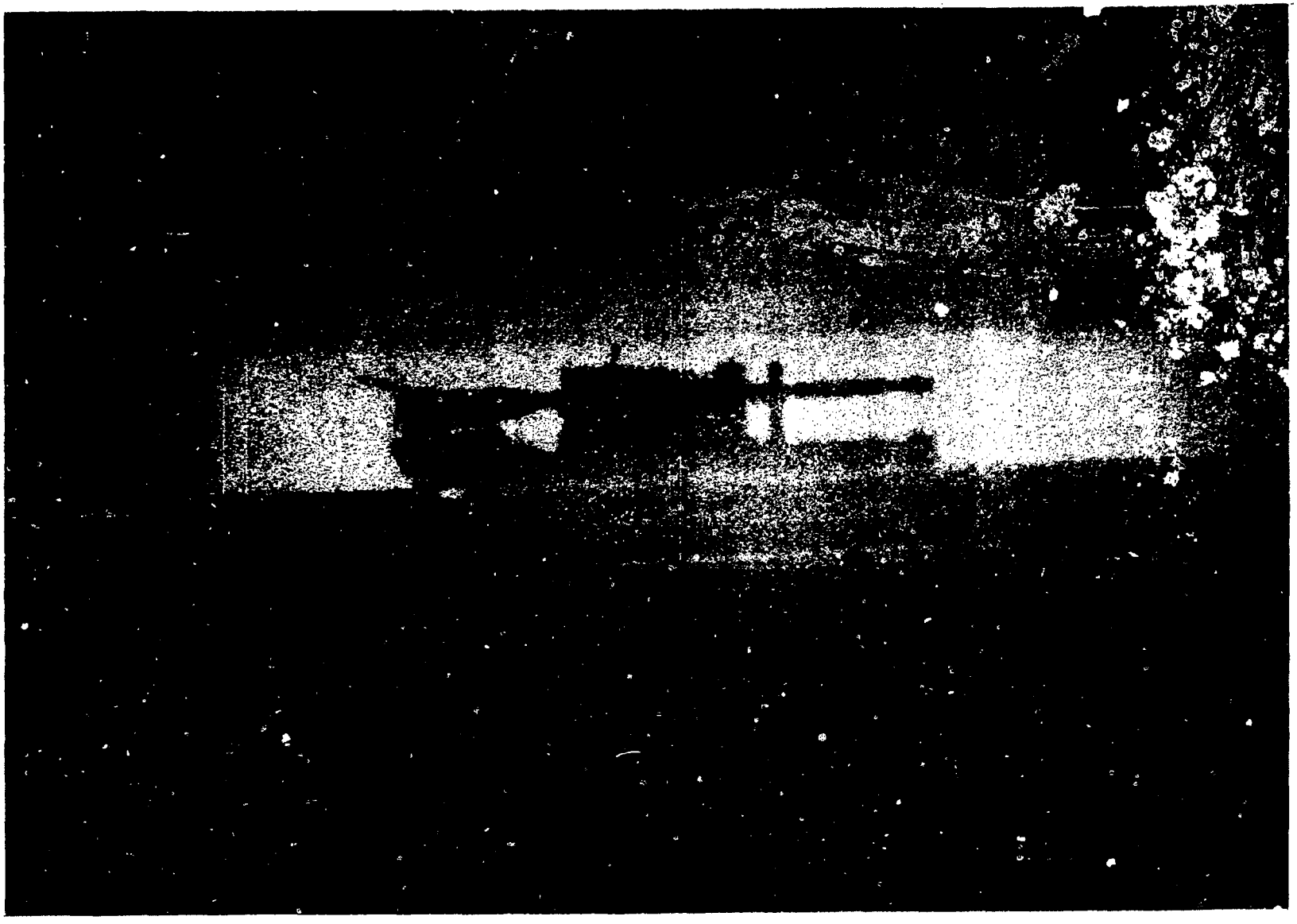

Figure III-6. Photograph of ship taken in the presence of a temperature inversion at 30 m.

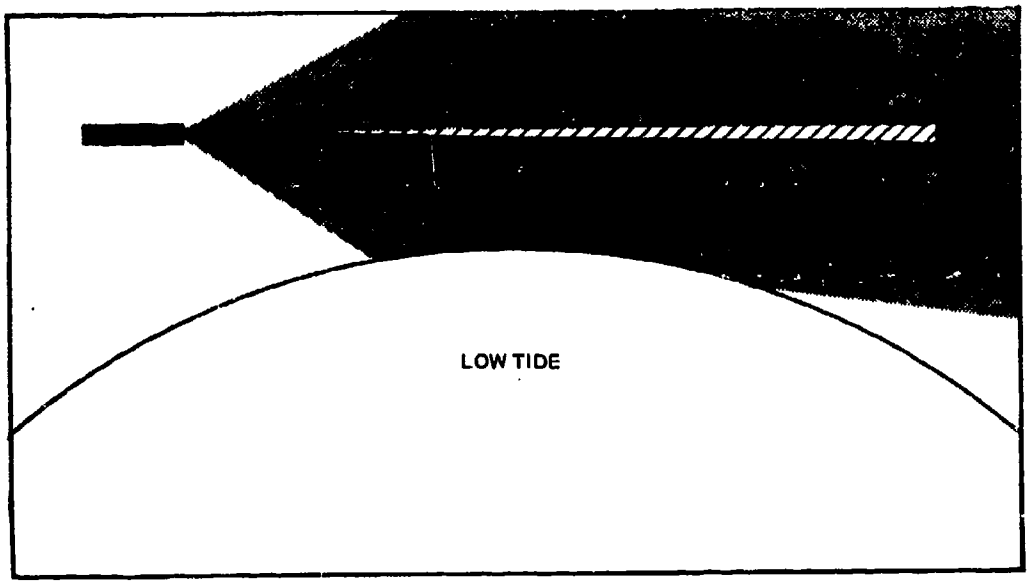

Figure III-7. Receiver in line of sight path of laser beam at low tide.

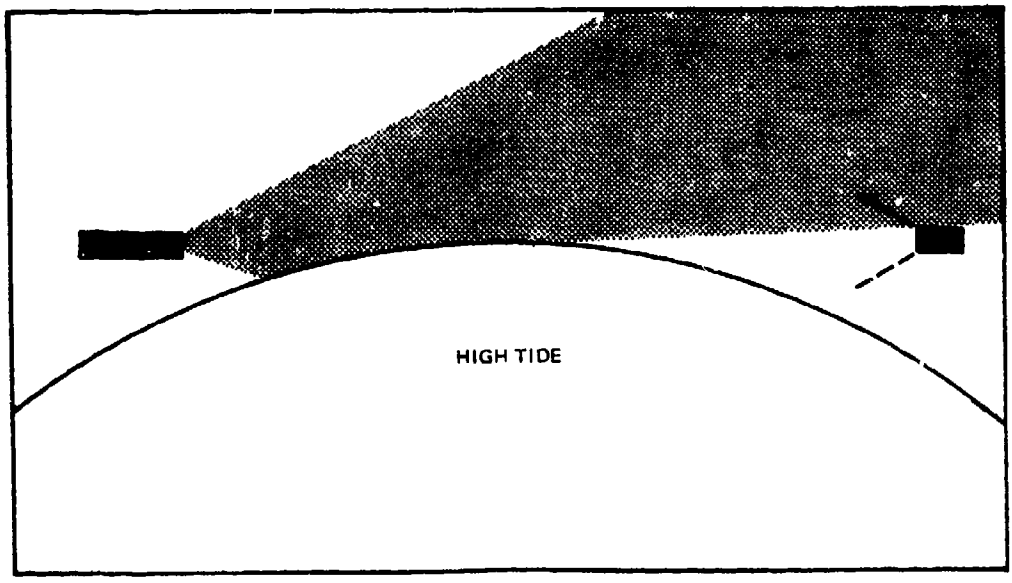

Figure III-8. Receiver in earth's shadow at high tide ($T_{sea} = T_{air}$).

tion for paths which remain above a height of about 1 metre, since the major portion of the air-sea temperature difference is accounted for within the first 10 cm beyond the interface.

As the tide rises, the sea surface interposes itself between the source and detector. If no strong refractive effects are present close to the surface ($T_s = T_a$), the beam would simply be extinguished when the source is eclipsed (Figure III-8). If however, there is a strong decrease in refractivity with height ($T_s < T_a$), the rays which pass close to the surface would be bent down around the earth reaching the detector (Figure III-9). Similarly, if there is a strong increase in refractivity with height ($T_s > T_a$), the rays passing close to the surface would be bent upward, causing loss of the signal sooner than expected (Figure III-10).

Therefore, by establishing an infrared transmission link close to the ocean surface and monitoring signal strength as a function of water height, the refractivity of the atmosphere just above the air-sea interface may be investigated.

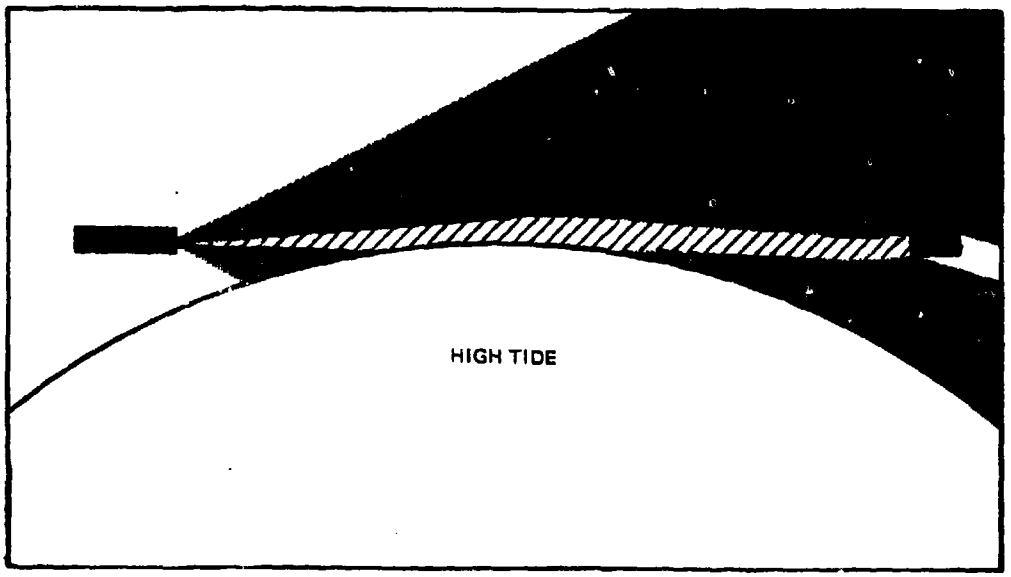

Figure III-9. Receiver in refracted laser beam at high tide ($T_{sea} < T_{air}$).

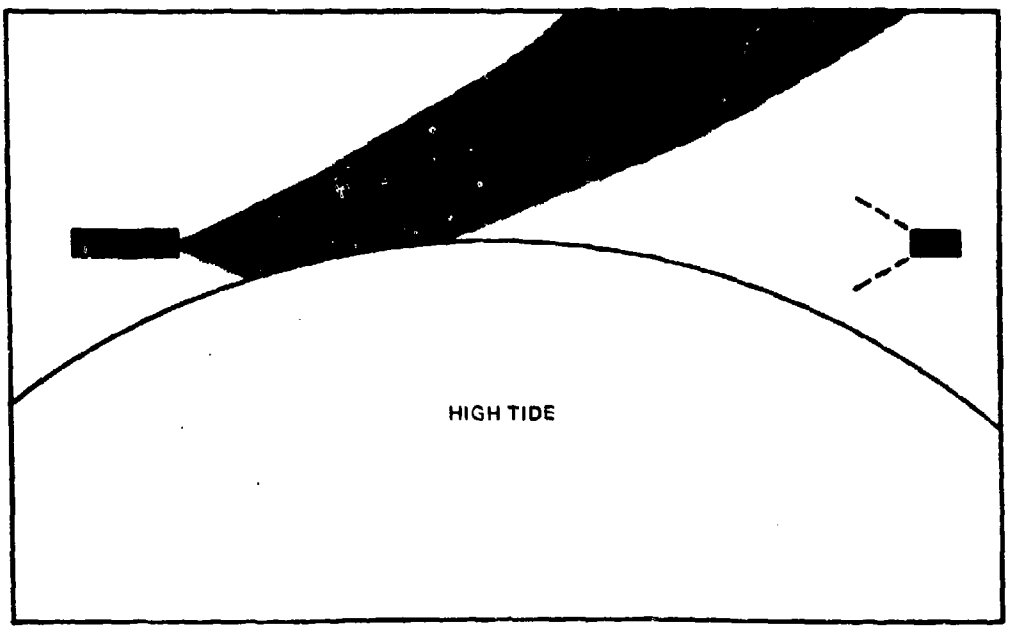

Figure III-10. Receiver below refracted laser beam at high tide ($T_{sea} > T_{air}$).

IV. DESCRIPTION OF CO_2 LASER TRANSMISSION EXPERIMENT

A. Transmission Path

In any experiment designed to measure small variations in the refraction of light, a long path length is desirable. In addition, the propagation medium should be as uniform as possible, with minimal effects due to wind or wave motions. For these reasons, as well as accessibility, we chose to conduct our measurements over an 8.5 km path stretching from southeast to northwest over San Diego Bay (Figure IV-1).

The laser transmitter was contained in a portable van. It was located on a sand spit at the San Diego Gas and Electric Plant in Chula Vista. The laser receiver and electronics were housed in an equipment hut situated on a concrete pier at the Naval Amphibious Base in Coronado. Since the path was out of the main channel, uninterrupted transmission could be maintained for long periods of time with minimum interference from boats.

B. Experimental Apparatus

1. General Description

The experimental apparatus is shown schematically in Figure IV-2. The infrared radiation emitted by a CO_2 laser was chopped and directed toward the receiving site. There, it was collected by a cassegrainian telescope and converted to an electrical signal by a pyroelectric detector. The chopper reference signal, which indicates when the chopper aperture is open or closed, was simultaneously transmitted by means of a microwave radio link. This allowed a lock-in amplifier to be used for synchronous detection of the laser signal, with a resultant increase in system sensitivity.

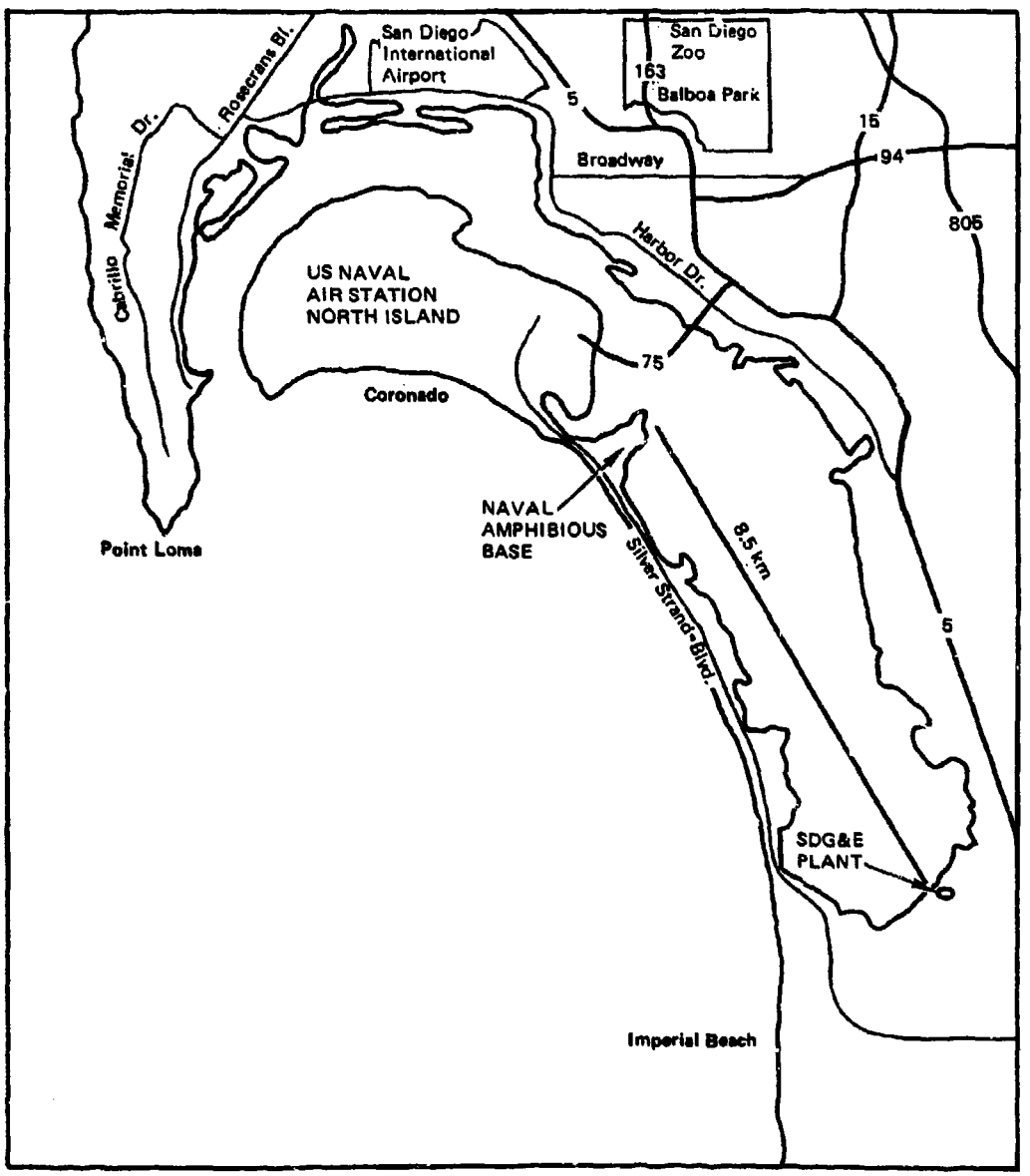

Figure IV-1. Transmission path over San Diego Bay for CO_2 laser transmission experiment.

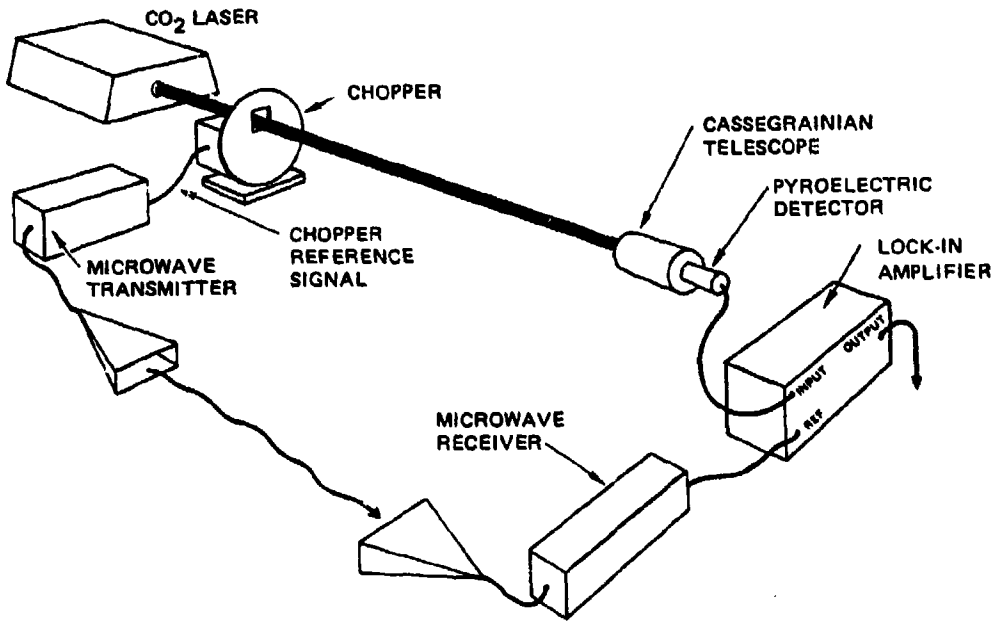

Figure IV-2. Schematic diagram of experimental apparatus.

2. Laser Transmitter

The main component of the laser transmitter was a GTE model 941S CO_2 laser. It radiated 3 watts CW at 10.6 μm with a long term amplitude stability of better than 5%. The CO_2 laser was rigidly mounted on an aluminum plate along with a Spectra-Physics model 132 2 mW helium-neon laser and a Weaver model T-16 16X gunscope (Figure IV-3).

The lasers and the gunscope were successively sighted in at 10 m, 200 m and 1 km. Small adjustments in their positions were made until the optical axes of all three were parallel. This arrangement facilitated aiming the CO_2 laser at the receiving site since it provided visual references for the operators on both ends of the path. When the receiving site was placed within the crosshairs of the gunscope, the helium-neon laser was easily visible to an observer at that location (even in the daytime).

In order to achieve good beam pointing stability, the laser plate was mounted across 3 inch I-beams which were bolted directly to the frame of the van. The van itself was raised on concrete blocks. No appreciable pointing jitter was noted.

The infrared laser beam was chopped at 40 Hz by a rotating blade chopper salvaged from a surplus Laser Precision model RKP-345 radiometer probe.

3. Laser Receiver

The chopped infrared radiation was collected by a Molectron model PT cassegrainian telescope. It had an effective focal length of 200 mm, an effective aperture number of f/2.8, and a full angular field of view of 1.42 degrees. The infrared radiation was detected by a Molectron model P4-45 pyroelectric detector. It was fitted with an anti-reflection coated germanium window in order to reject background light outside the 8-14 μm band. The responsivity of the detector was on the order of 10^4 volts/watt.

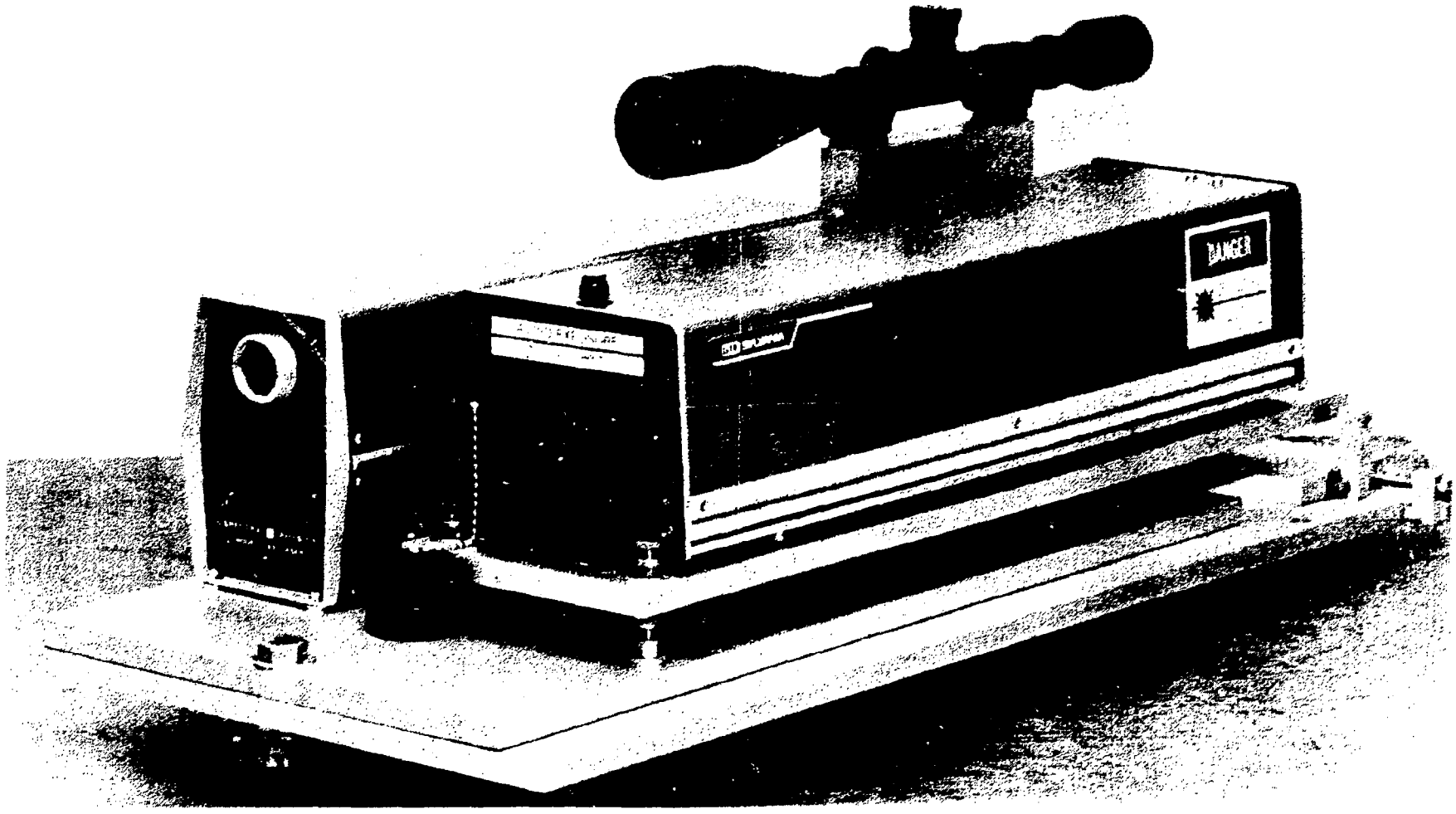

Figure IV-3. Photograph of CO_2 laser, He-Ne laser, and gunscope mounted on aiming plate.

The electrical signal from the detector was monitored by a Princeton Applied Research model 5204 lock-in analyzer in the vector voltmeter mode. The magnitude of signal was observed on a front panel meter and continuously recorded on a Mosely model 680 strip chart recorder.

The telescope-detector combination was mounted on an adjustable tilt-plate which could be located on any desired support at the receiving site. In Figure IV-4, it is shown in place on a specially constructed platform which suspended the assembly close to the ocean surface.

4. Microwave Reference Link

In order to employ synchronous detection, it was necessary to provide a chopper reference signal to the lock-in amplifier. This was done by means of the microwave reference link shown in Figure IV-5.

A 2.9 GHz Fairchild phase-locked oscillator was amplified to about 0.5 watt by a Hewlett-Packard model 491C traveling wave amplifier. The TWA was modulated by the chopper reference signal and fed to a 20 dB gain microwave horn for transmission.

The signal was received by a similar horn, amplified by an EM Labs model 2900 preamplifier, and then fed to a Microtel model 1200 frequency tracking receiver. The chopper signal was extracted from the carrier with a Hewlett-Packard model 423A diode detector and processed with a comparator amplifier in order to produce a clean reference signal for the lock-in amplifier.

C. Meteorological Measurements

During the course of a run, the following met measurements were made at the receiver site. Air and sea temperatures were measured to within $\pm 0.1^{\circ}C$ using thermometers. The air temperature was generally measured at about 2 m above

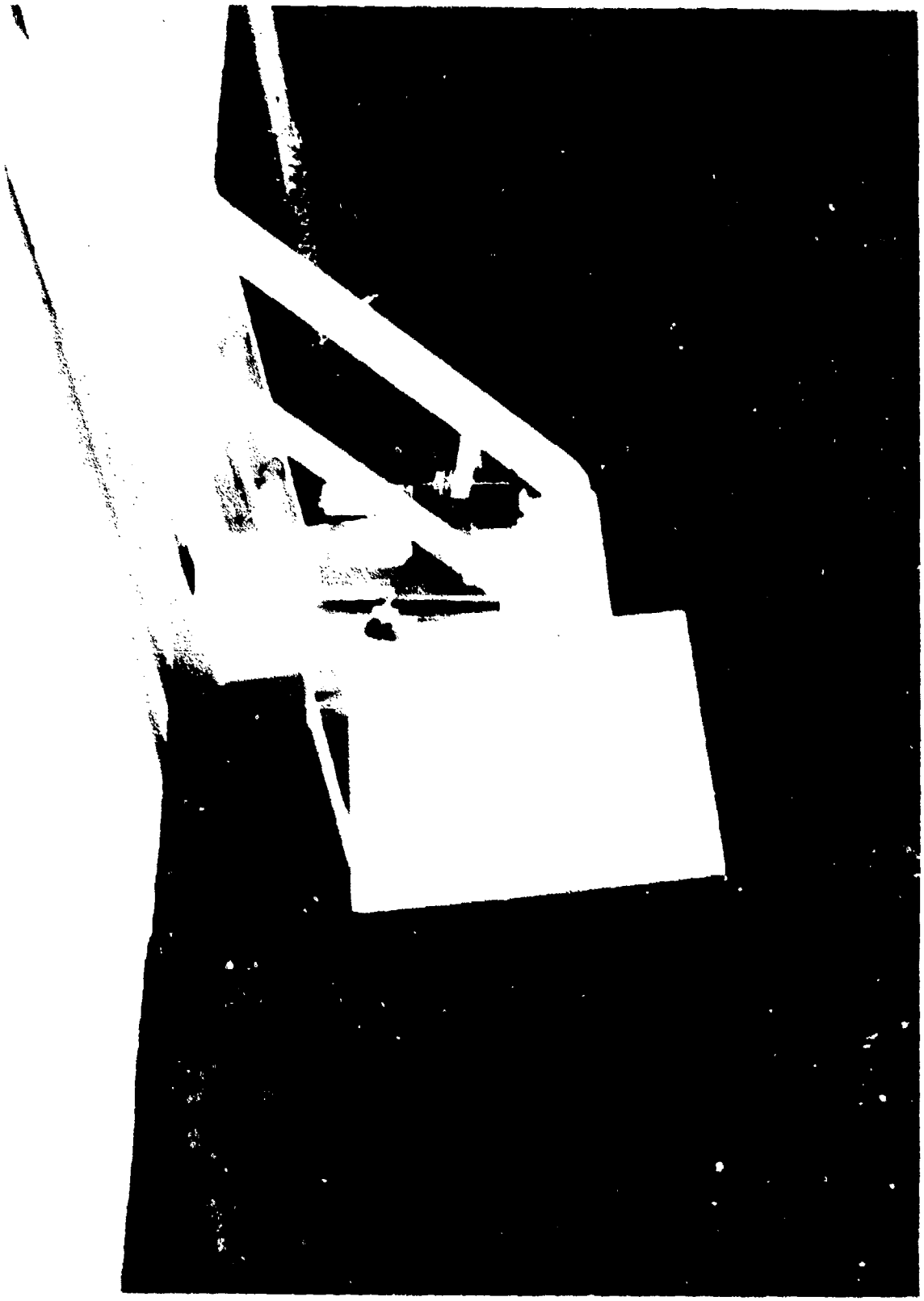

Figure IV-4. Photograph of telescope-detector combination suspended close to the ocean surface.

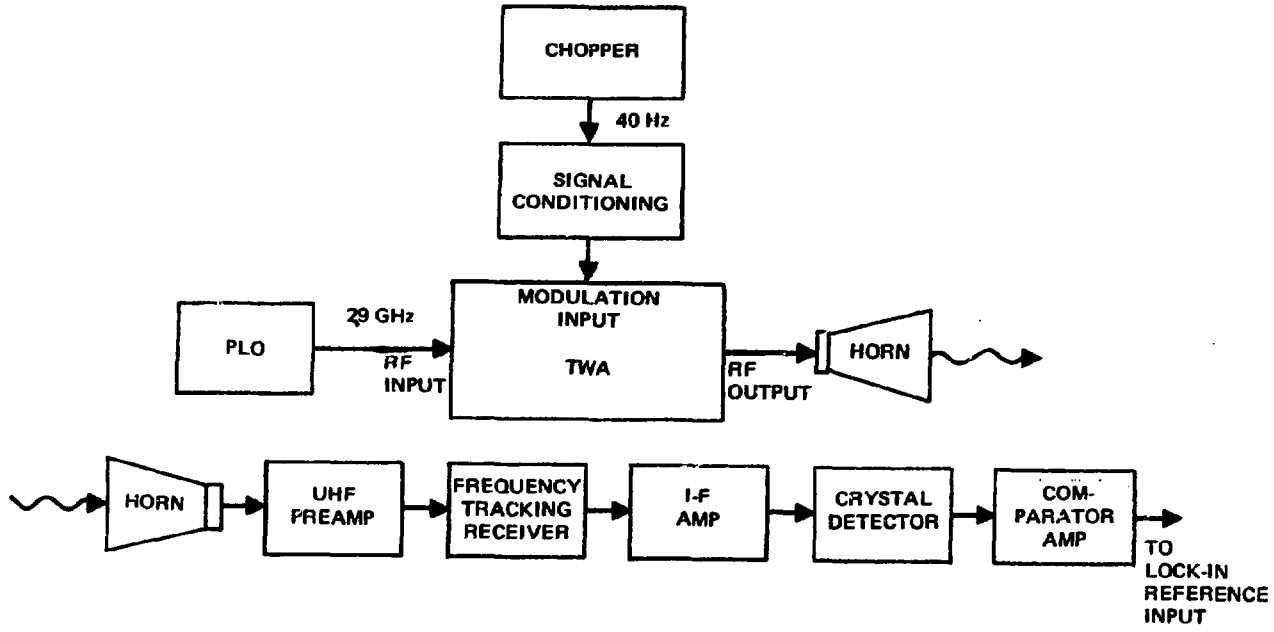

Figure IV-5. Schematic diagram of microwave reference link.

the ocean surface. Wind speed was measured to within about ±2 mph using a hand held instrument. The height of the detector above the water line was measured to within about ±5 cm using a dipstick.

D. Measurement Procedure

Each time data were taken, measurements were made in the following manner. The microwave horns were set up and coarsely pointed at the opposite site. The telemetry was then turned on and reception of the reference signal verified.

The helium-neon laser was then turned on. In general, it was visible at some height at the receiving site which was dependent on the meteorological conditions and the tide. Realignment of the laser plate was usually not attempted unless the beam was not visible at all.

An eyepiece was substituted for the pyroelectric detector in order to visually align the collector telescope. The detector was replaced and the CO_2 laser turned on. Since the beam divergence of the helium-neon laser was 1 mr and that of the CO_2 laser was 4 mr, the infrared signal was almost always observed after this process. The lock-in amplifier was run with a time constant of 100 seconds in order to smooth out signal fluctuations. Meteorological measurements were made at the receiving site approximately every half hour during the run.

V. DATA

A. General Behavior

Over the course of three months, data was taken on eighteen separate days. During all days but the first, the detector had to be located significantly higher than would be expected for line of sight contact in the standard atmosphere. Throughout these runs, the sea temperature generally exceeded the air temperature by several degrees centigrade.

For data taken during a rising tide (Figure V-1), the laser signal (while it was detectable) exhibited no sharp fades or fluctuations. As the tide rose and contact was lost, the signal dropped several orders of magnitude in just a few minutes. When this occurred, the detector was raised up until the signal was again acquired. The procedure was repeated until high tide was reached. Data taken during falling tides (Figure V-2) was similar except that the detector was successively lowered each time the signal emerged from the background.

B. Analysis

Let an optical source at height h_s and a receiver at a different height h_r be separated by a distance R. Further, as shown in Figure V-3, let the source and receiver be positioned so that their optical horizon distances d_s and d_r respectively, coincide. Therefore $d_s + d_r = R$ and at this point, the source is just detectable by the receiver. The distance to the optical horizon, d_o, as seen by an observer at height h_o through a refractive index gradient dn/dh is given by (Reed and Russell, 1964)

$$d_o = \sqrt{\frac{2ah}{1+a(dn/dh)}} \qquad (1)$$

where a is the radius of the earth.

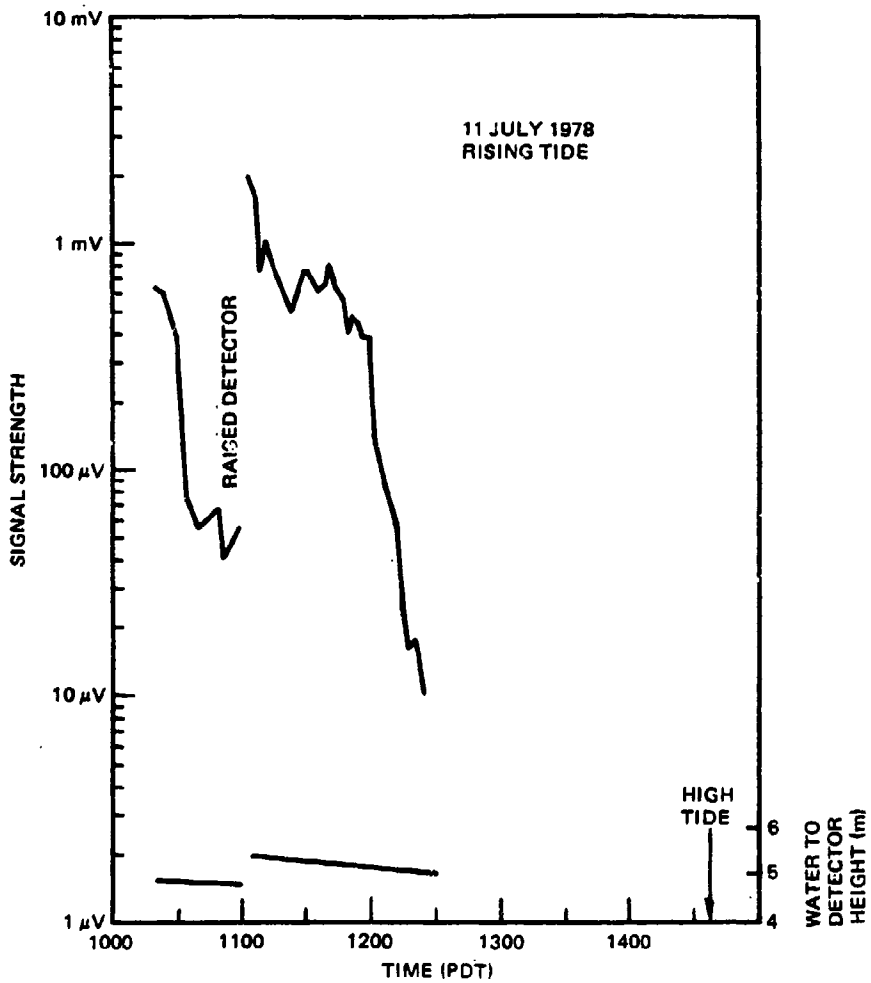

Figure V-1. Example of received signal vs. time during a rising tide.

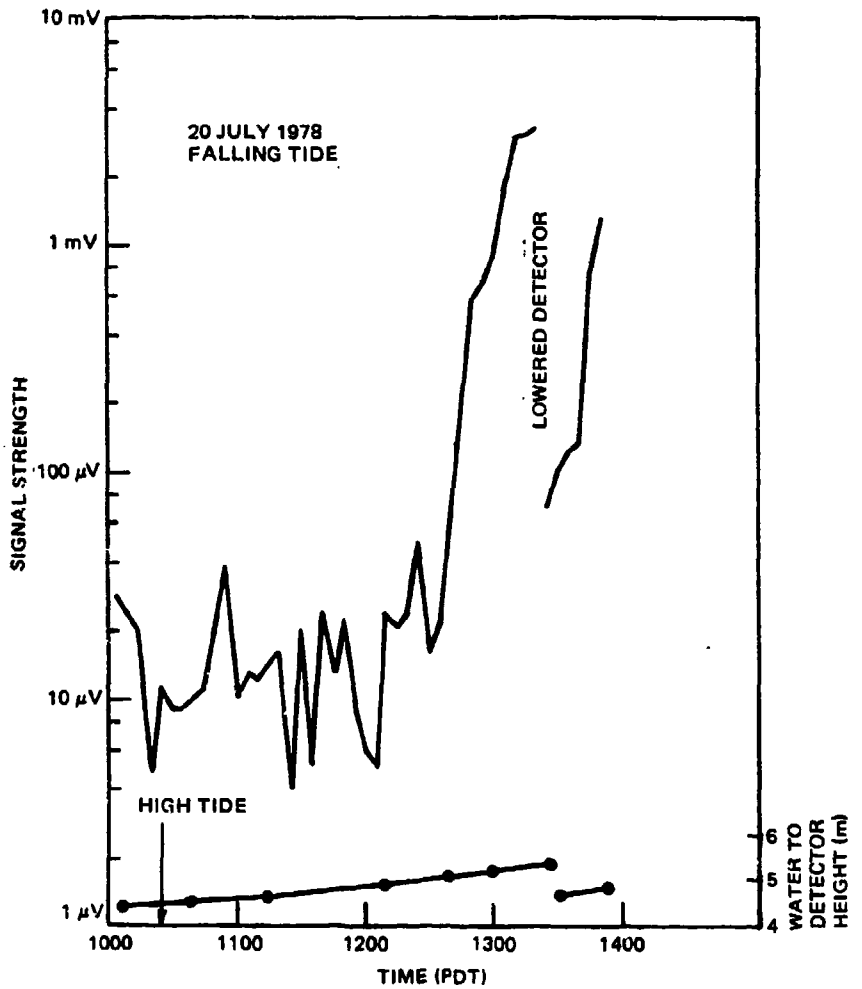

Figure V-2. Example of received signal vs. time during a falling tide.

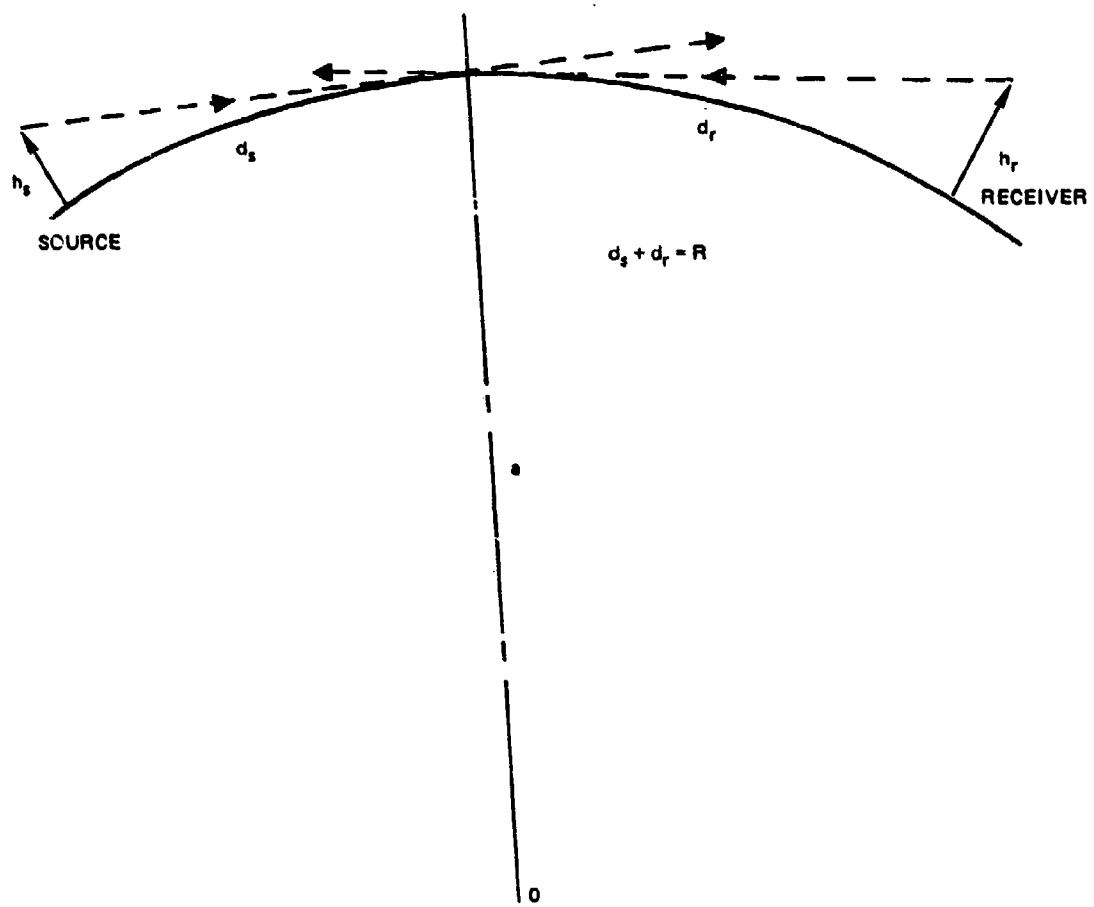

Figure V-3. Diagram of horizon distances for source and receiver at heights h_s and h_r respectively.

Then from (1)

$$d_s = k\sqrt{h_s} \tag{2a}$$

and $$d_r = k\sqrt{h_r} \tag{2b}$$

where $$k = \sqrt{\frac{2a}{1+a(dn/dh)}} \tag{3}$$

or $$d_s + d_r = R = k\,(\sqrt{h_s} + \sqrt{h_r}) \tag{4}$$

If R is fixed, h_s and h_r may be experimentally determined from the water height at the time the observer just loses sight of the source. Then the horizon distance for an observer at any height h_o (for the same linear refractive index gradient as for which h_s and h_r were measured) is given by

$$d_o = \left(\frac{R}{h_s + h_r}\right)\sqrt{h_o} \tag{5}$$

where the units of d_o are those of R.

The values of h_s and h_r measured during 14 different eclipses or appearances of the signal, along with the corresponding values of k are shown in Table V-1. Also shown are the corresponding values of measured sea and air temperature (air temperature measured at fixed height on pier). With the exception of 3 events, the air temperature was always less than the sea temperature (these are end-point measurements and are probably not representative of average values over the path).

The average value of k for the 14 events is 2.15 $km/\sqrt{m}$. Then from (3) the refractive index gradient can be determined to be $2.76 \times 10^{-7}\ m^{-1}$. From equation (III-3) the temperature gradient corresponding to this gradient of refractive index is

$$\frac{\partial T}{\partial z} \approx -\frac{T}{N}\left(\frac{\partial n}{\partial z}\right) \times 10^6 \tag{6}$$

where N is given by III-2. The average value of T for the data set is $22.7^{\circ}C$. For the measured values $\partial T/\partial z \approx -.3^{\circ}C$/metre.

Table V-1

Date	T_{sea} (^{o}C)	T_{air} (^{o}C)	h_s (m)	h_r (m)	k $km\text{-}m^{-\frac{1}{2}}$
11 Jul	21.7	19.9	3.66	4.89	2.07
11 Jul	22.1	20.0	3.24	5.13	2.10
12 Jul	22.0	21.7	3.47	4.70	2.12
13 Jul	23.2	24.8	3.09	4.32	2.23
17 Jul	23.3	18.8	3.55	4.78	2.10
20 Jul	22.7	21.9	3.26	5.15	2.10
20 Jul	22.6	21.9	3.55	4.78	2.10
21 Jul	22.7	20.2	3.02	4.91	2.16
24 Jul	22.2	22.3	3.02	4.24	2.25
27 Jul	22.9	21.5	3.24	4.47	2.18
28 Jul	23.2	21.9	3.24	4.47	2.18
4 Aug	23.6	23.8	3.40	4.63	2.14
23 Aug	23.2	21.5	2.94	4.83	2.19
23 Aug	23.1	21.8	3.17	4.40	2.20

The distance to the geometrical horizon is found from (1) for dn/dh=0 to be $d_g = 3.57\sqrt{h}$

where h is in metres and d is in kilometres. The results of this study show that for negative temperature gradients of a few tenths of a degree centrigrade, the distance to the infrared (or optical) horizon ($d_o \approx 2.15\sqrt{h}$) is only about 60% of the distance to the geometrical horizon.

The distance to the optical horizon for a wide range of temperature and index gradients is shown in Figure V-4. It is evident that the horizon shortens relatively slowly for temperature gradients more negative than that of the standard atmosphere. For positive gradients however, the corresponding increase in horizon distance is much more rapid. This indicates that temperature gradients of similar magnitude but opposite sign to those observed in this experiment would result in greatly extended horizons.

Listed in Appendix C is a computer program called RAYPROP. It may be used to compute the various parameters related to a source or observer's horizon for a constant gradient of index of refraction.

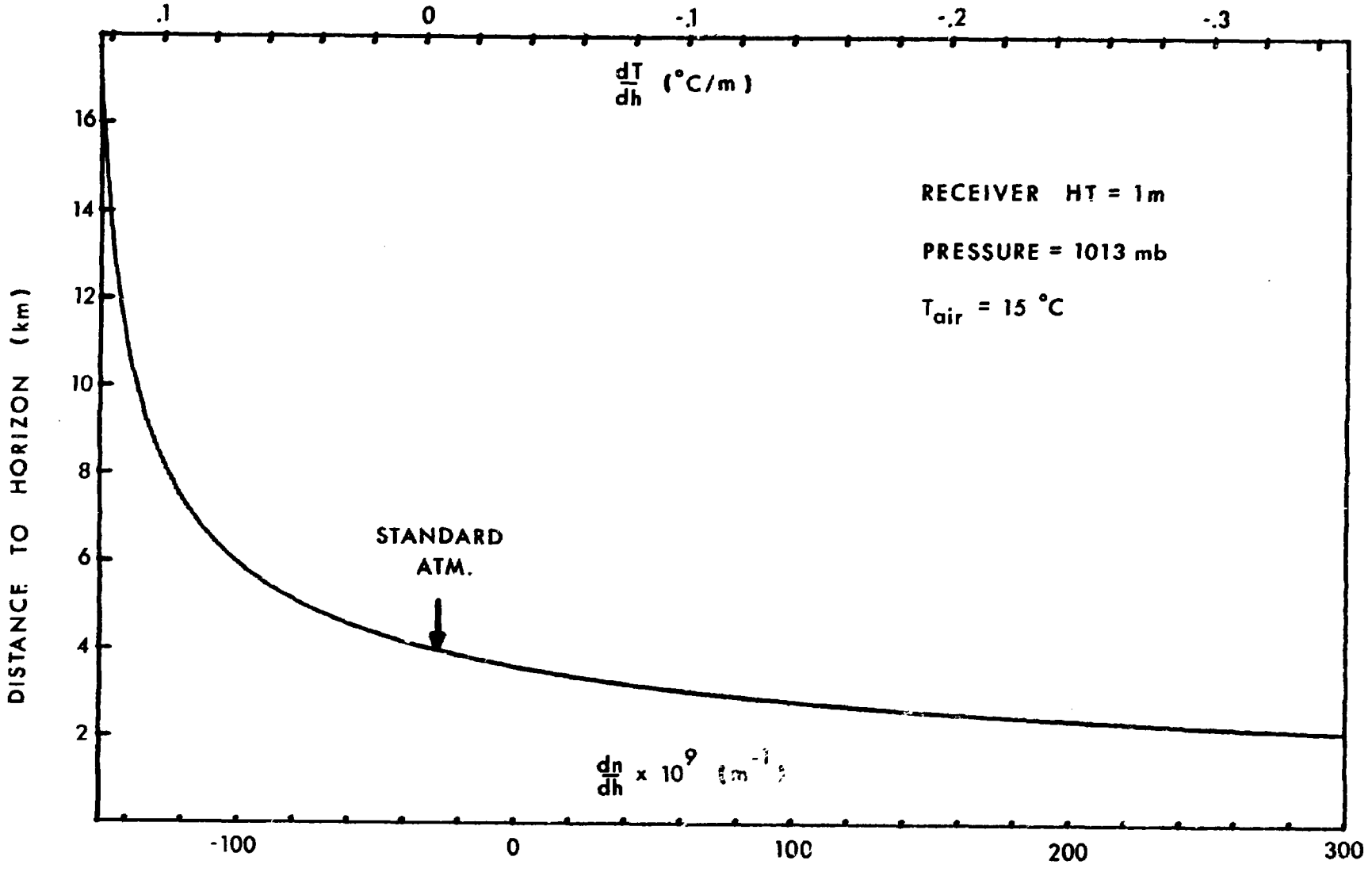

Figure V-4. Distance to the horizon vs. index gradient and temperature gradient for an observer at a height of 1 m.

VI. CONCLUSIONS AND RECOMMENDATIONS

Because of the prevailing meteorological conditions which existed in San Diego Bay during the measurement period, this study was limited to data acquired when the bay water was warmer than the air. For air temperature gradients less than $-1^{\circ}C/m$, it was demonstrated that a severe shortening of the optical and infrared horizons consistently occur. Also, calculations indicate that if gradients of similar magnitude but of opposite sign occur close to the ocean surface, greatly extended horizons are to be expected. However, most of the advantages gained by extended horizons could be nullified by the effects of absorption due to water vapor. In any case, since in many of the Navy's operational areas (especially during winter) the sea is warmer than the air, the detrimental effects of shortened horizons and distorted images are more likely to be encountered.

In addition to the above effects to be expected on passive surveillance devices, laser systems (target designators and trackers) operated close to the ocean surface could be subject to large errors in pointing and tracking. This could result from strong refractivity gradients which exist near the air-sea interface.

The quantitative studies made here have been limited to infrared wavelengths propagating close to the ocean surface. However, the visual evidence presented indicates that elevated ducts could also cause severe image distortions for imaging systems operated at other heights (aircraft, ship mast, etc.).

Based on the results of this study, it is recommended that a climatological data base of air-sea temperature differences for operational areas be assembled. This would aid shipboard commanders in assessing the effects of refractivity gradients on electro-optical systems' performance. For example, a library could

be developed to ascertain the distance to the horizon for a particular shipboard electro-optical system at any location and time of year.

Real time, shipboard optical refractivity sensors also need be developed to enhance predictive capabilities. The computer programs developed in this investigation provide a means of predicting image distortion in the presence of refractivity gradients. These programs, in conjunction with real time meteorological measurements, would enable simulated images of expected targets to be displayed. This would aid electro-optical systems operators in identifying targets under degraded optical conditions.

REFERENCES

1. FLEAGLE, R. G., "The Optical Measurement of Lapse Rate", Bull. Amer. Met. Soc., 31, 51 (1950)
2. FLEAGLE, R. G., "The Temperature Distribution Near a Cold Surface", Jour. of Met., 13, IGO (1956)
3. FLEAGLE, R. G. and BUSINGER, J. A., "An Introduction to Atmospheric Physics", Academic Press, CHAPTER VII, (1963)
4. KERR, D. E., "Propagation of Short Radio Waves", McGraw-Hill (1951)
5. REED, H. R. and RUSSELL, C. M.", "Ultra High Frequency Propagation", Boston Technical Publishers, Chapter 3, (1964)
6. SELBY, J. E. A., SHETTLE, E. P. and MC CLATCHEY, R. A., "Atmospheric Transmittance from .25 to 28.5 μm: Supplement Lowtran 3B (1976)", AFGL, Paper No. AFGL-TR-76-0258

APPENDIX A

COMPUTER PROGRAM RAYTRACE

This appendix describes a FORTRAN computer program that calculates and displays ray trajectories for arbitrary but piecewise linear modified refractivity versus height profiles.

Program RAYTRACE is a FORTRAN IV program designed for use on the Data General Nova 800 minicomputer system using the operating system RDOS. Both input and output of the program is via the Tektronix 4012 interactive graphics display terminal. The purpose of the program is to calculate and display ray trajectories on a height-versus-range plot for an arbitrary but piecewise linear refractivity-versus-height profile. Other inputs to the program are: maximum range, range increment, maximum height, source height, initial launch angle, final launch angle, and number of rays. The program uses Snell's law with small angle approximations to compute the ray trajectories based on an input modified refractivity profile specified in M-units. Modified refractivity in M-units is related to refractivity in N-units by the relation

$$M = N + 0.048\ h$$

where h is in feet. This appendix will not attempt to explain the inner workings of the program or the formulations employed, but rather will outline the operation of the program.

Figure A-1 shows a sample of the prompt and input sequence for entering the modified refractivity profile that occurs at the beginning of the program. Note that the required levels must be entered in order of descending height and must end at the zero height level. A maximum of 50 levels may be entered. After the zero height level has been entered, the program clears the screen, plots the M-units versus height, and prompts for the remaining inputs as illustrated by the example of Figure A-2. All of the remaining inputs are self explanatory except,

```
INPUT PROFILE FROM HIGHEST TO LOWEST WITH THE FORM
HEIGHT(FEET), M UNITS

? 164.0,279.0
? 98.4,276.5
? 65.3,279.5
? 0.0,276.0
```

Figure A-1. Sample Prompt and Input Sequences for Entering the Modified Refractivity Profile.

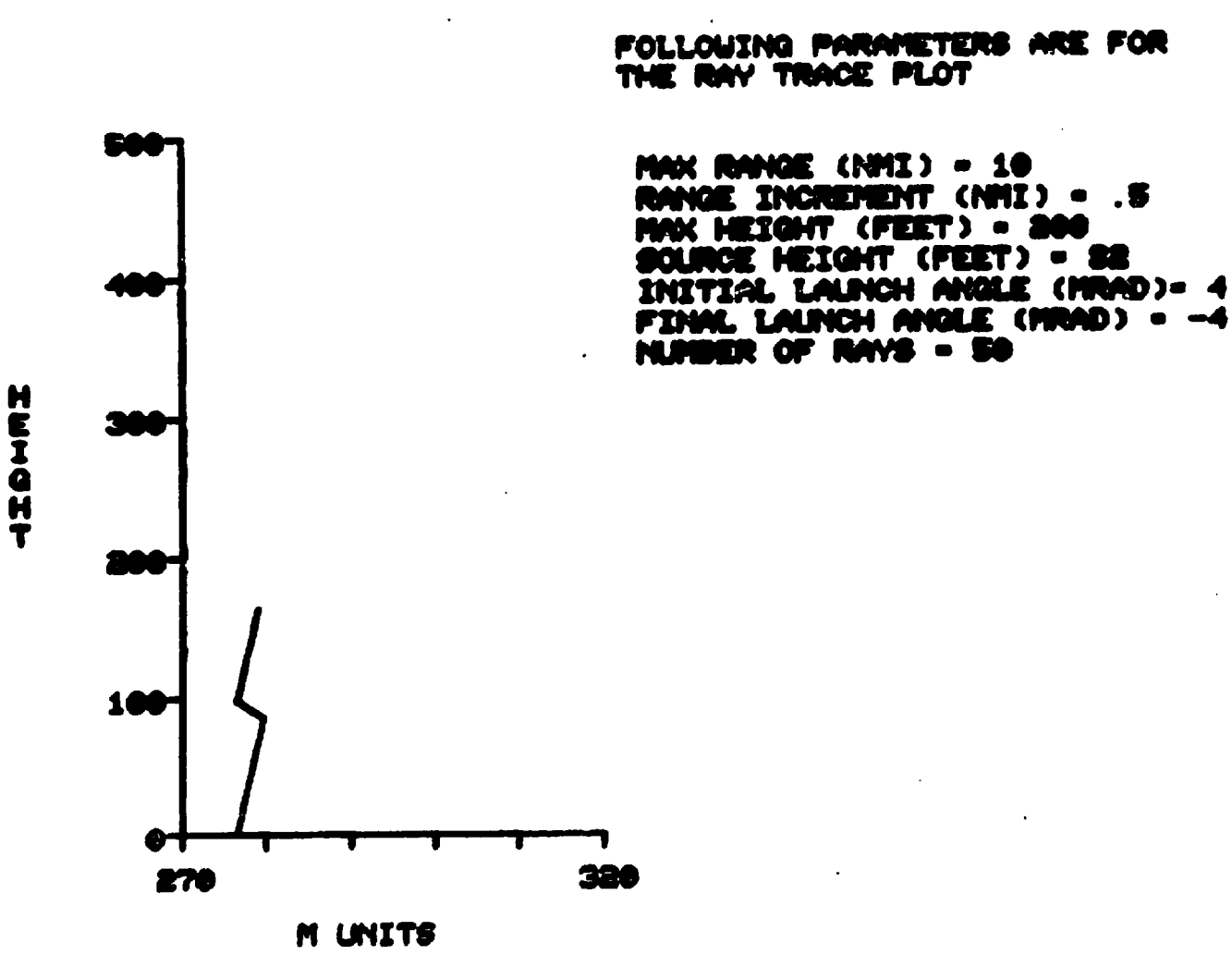

Figure A-2. Sample Modified Refractivity Plot vs Height. Also shown are the Prompt and Input Sequences for the Remaining Inputs Needed to Generate a Ray Trace Plot.

perhaps, the range increment which should be selected based on the maximum range and the complexity of the M-unit profile to give smoothly curving ray trajectories Under most conditions a range increment of one-twentieth the maximum range is a good choice.

Figure A-3 shows the final ray trace plot for the inputs shown in Figures A-1 and A-2. After each ray trace plot is generated, an entry of "O" (for Old Profile followed by a carriage return will direct program flow to the entries illustrated in Figure A-2. An entry of "N" (for New Profile) followed by a carriage return, will direct program flow to the M-unit profile inputs illustrated in Figure A-1.

A complete FORTRAN program listing of program FAYTRACE and the one subroutine TRACE are included here following the figures.

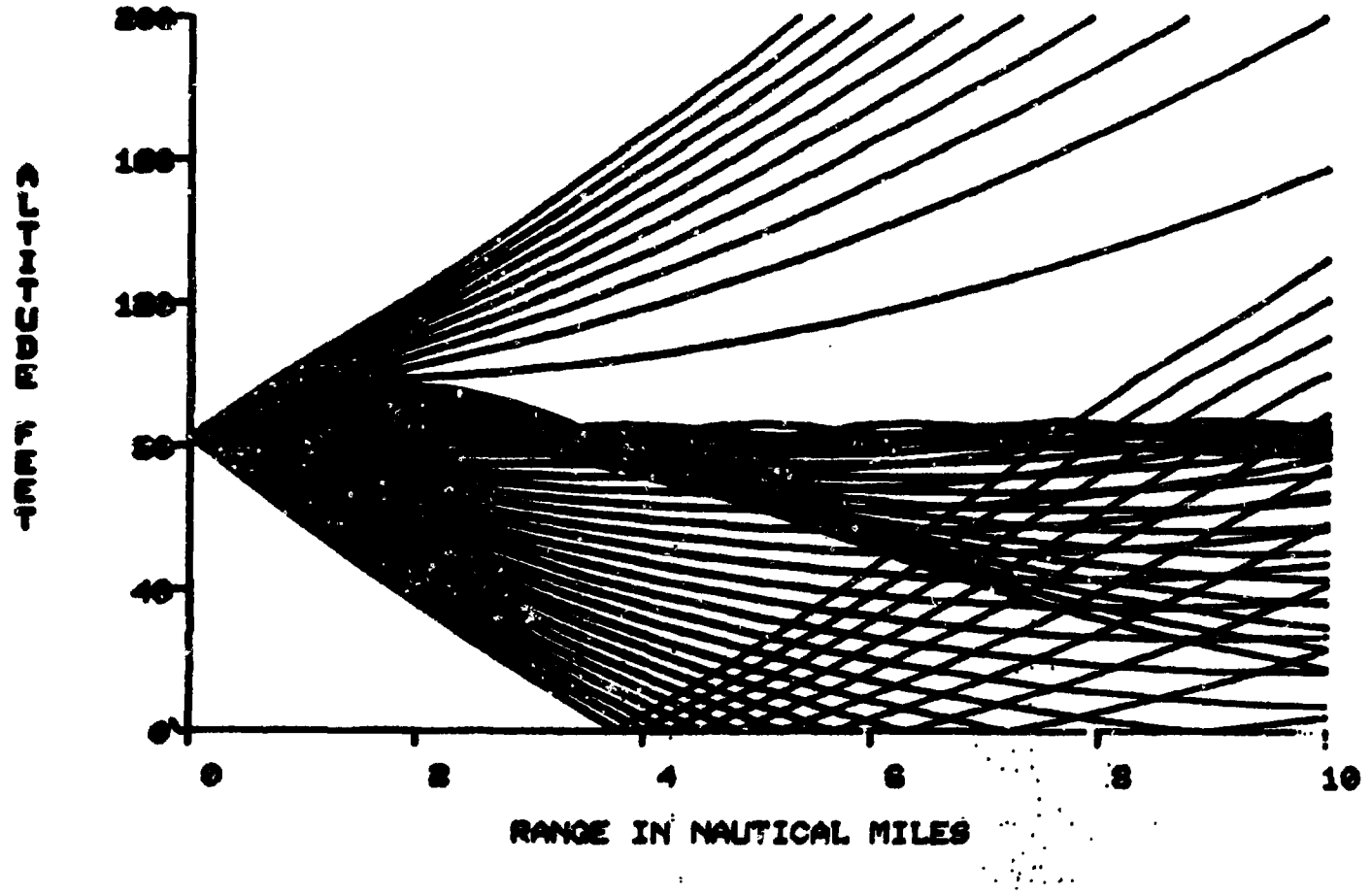

Figure A-3. Sample Ray Trace Plot for the Inputs Specified in Figures A-1 and A-2.

```
C     PROGRAM RAYTRACE
      COMMON/A/ H(50),RM(50),DMLIM(6),HLIM(7),LBL(6),LBA(13)
      COMMON/B/ QA(50),YA(50),NMAX
      DATA DMLIM/50.,100.,200.,500.,1000.,2000./,
     1     HLIM/500.,1000.,2000.,5000.,10000.,20000.,40000./,
     2    LBL/'H',' ','I','G','H','T'/,
     3    LBA/'A','L','T','I','T','U','D','E',' ','F','E','E','T'/
      CALL INITT(480)
    5 TYPE "INPUT PROFILE FROM HIGHEST TO LOWEST WITH THE FORM<15>",
     1"HEIGHT(FEET), M UNITS <15>","<15>"
      DO 10 I=3,50
      ACCEPT " = ",H(I),RM(I)
      IF(H(I).EQ.0.0) GO TO 20
   10 CONTINUE
      TYPE " PROFILE ARRAY FULL  RE-ENTER PROFILE"
      GO TO 5
C     PROFILE READ IN COMPLETE  SCALE PROFILE FOR PLOTTING
   20 NMAX=I
      RMMIN = RM(NMAX)
      RMMAX = RMMIN
      DO 25 I=3,NMAX
      RMI = RM(I)
      IF(RMI.LT.RMMIN) RMMIN=RMI
      IF(RMI.GT.RMMAX) RMMAX=RMI
   25 CONTINUE
      DELM = RMMAX-RMMIN
      DO 30 I=1,5
      IF(DELM.LT.DMLIM(I)) GO TO 35
   30 CONTINUE
      I=5
   35 DM = DMLIM(I)                          ;TOTAL M CHANGE ON AXIS
      RMMIN = RMMIN-AMOD(RMMIN,DM/5.) ;MINIMUM M ON AXIS
      HMAX=H(3)
      DO 40 I=1,7
      IF(HMAX.LE.HLIM(I)) GO TO 45
   40 CONTINUE
      I=7
   45 HMAX=HLIM(I)
C DRAW VERTICAL AXIS
   47 CALL NEWPAG
      IY=200
      CALL MOVABS(190,100)
      CALL DRWABS(200,100)
      DO 50 I=1,5
      CALL DRWABS(200,IY)
      CALL DRWABS(190,IY)
      CALL MOVABS(200,IY)
   50 IY=IY+100
C DRAW HORIZONTAL AXIS
      CALL MOVABS(200,90)
      CALL DRWABS(200,100)
      IX=260
      DO 60 I=1,5
      CALL DRWABS(IX,100)
      CALL DRWABS(IX,90)
      CALL MOVABS(IX,100)
   60 IX=IX+60
C PLOT M VERSUS HEIGHT
      UPM=300./DM     ;SCREEN UNITS PER M UNIT
      UPH=500./HMAX   ;SCREEN UNITS PER FOOT
      IX = 200+(RM(3)-RMMIN)*UPM
      IY = 100+H(3)*UPH
      CALL MOVABS(IX,IY)
      DO 70 I=4,NMAX
      IX = 200+(RM(I)-RMMIN)*UPM
      IY = 100+H(I)*UPH
   70 CALL DRWABS(IX,IY)
      IY=410
      DO 75 I=1,6
      CALL MOVABS(80,IY)
      CALL ANMODE
```

```
      WRITE(10,10C) LBL(I)
   75 IY=IY-20
  100 FORMAT(1X,A1)
      IY=590
      IHLABEL = HMAX
      IHINC = HMAX/5
      DO 80 I=1,6
      CALL MOVABS(12C,IY)
      CALL ANMODE
      WRITE(10,12C) IHLABEL
      IY=IY-100
   80 IHLABEL = IHLABEL-IHINC
  120 FORMAT(1X,I5)
      CALL MOVABS(170,60)
      CALL ANMODE
      MMIN=PMMIN
      MMAX=PMMIN+DM
      WRITE(10,14C) MMIN
  140 FORMAT(1X,I4)
      CALL MOVABS(470,60)
      CALL ANMODE
      WRITE(10,14C) MMAX
      CALL MOVABS(200,20)
      CALL ANMODE
      WRITE(10,16C)
  160 FORMAT(7X,'M UNITS',//////' FOLLOWING PARAMETERS ARE FOR',/' THE R
     1AY TRACE PLOT'//)
      ACCEPT " MAX RANGE (NMI) = ",RMAX," RANGE INCREMENT (NMI) = ",
     1 DELR," MAX HEIGHT (FEET) = ",HRMAX,
     2 " SOURCE HEIGHT (FEET) = ",HSOURCE," INITIAL LAUNCH ANGLE (MRAD)
     3= ",ALPHAS," FINAL LAUNCH ANGLE (MRAD) = ",ALPHAT," NUMBER OF RAYS
     4 = ",NRAYS
C SCALE PROFILE FOR RAYTRACE PLOT
      SX = 800/RMAX
      SY=500/HRMAX
      SYOSX2 = SY/SX**2
      YA(1) = 500.
      YA(2) = 500.
      YA(3) = H(3)*SY
      QA(2) = 0.
      QA(3) = 3.6E-8*SYOSX2
      DO 210 I=4,NMAX
      YA(I) = H(I)*SY
  210 QA(I) = (RM(I-1)-RM(I))/(H(I-1)-H(I))*SYOSX2*1.E-6
      SYOSX = SY/SX
      AS = ALPHAS*SYOSX*1.E-3
      AT = ALPHAT*SYOSX*1.E-3
      YS = HSOURCE*SY
      DELA = (AS-AT)/(NRAYS-1)
      AL = AS
      DR=DELR*SX
      DO 215 I=1,NMAX
      J=NMAX-I
      IF(YS.LT.YA(J)) GO TO 217
  215 CONTINUE
  217 KS=J+1
C DRAW VERTICAL RAYTRACE AXIS
      CALL NEWPAG
      CALL MOVABS(140,100)
      CALL DRWABS(150,100)
      IY=200
      DO 220 I=1,5
      CALL DRWABS(150,IY)
      CALL DRWABS(140,IY)
      CALL MOVABS(150,IY)
  220 IY=IY+100
      IY=480
      DO 230 I=1,13
      CALL MOVABS(30,IY)
      CALL ANMODE
      WRITE(10,31C) LBA(I)
  230 IY=IY-20
```

```
  310 FORMAT(1X,A1)
      IY=590
      IHLABEL=HRMAX
      IHINC=HRMAX/5.
      DO 240 I=1,6
      CALL MOVABS(70,IY)
      CALL ANMODE
      WRITE(10,120) IHLABEL
      IY=IY-100
  240 IHLABEL = IHLABEL-IHINC
C DRAW HORIZONTAL RAYTRACE AXIS
      CALL MOVABS(150,90)
      CALL DRWABS(150,100)
      IX=310
      DO 250 I=1,5
      CALL DRWABS(IX,100)
      CALL DRWABS(IX, 90)
      CALL MOVABS(IX,100)
  250 IX = IX+160
      CALL MOVABS(380, 20)
      CALL ANMODE
      WRITE(10,320)
  320 FORMAT(1X,'RANGE IN NAUTICAL MILES')
      IR=0
      IRINC=RMAX/5.
      IX=120
      DO 260 I=1,6
      CALL MOVABS(IX, 60)
      CALL ANMODE
      WRITE(10,330) IR
      IR = IR+IRINC
  260 IX=IX+160
  330 FORMAT(1X,I4)
C TRACE ALL RAYS
      DO 270 I=1,NRAYS
      CALL TRACE(YS,0.,AL,DR,KS)
  270 AL = AL-DELA
      CALL MOVABS(900,0)
      CALL ANMODE
      READ(11,500) IOPT
  500 FORMAT(A1)
      CALL NEWPAG
      IF(IOPT.EQ.'N') GO TO 5
      IF(IOPT.EQ.'O') GO TO 47
      CALL FINITT(0,800)
      END
      SUBROUTINE TRACE(YS,XS,AS,DX,KS)
      COMMON/B/QA(50),YA(50),NMAX
      IX=XS
      IY=YS
      CALL MOVABS(IX+150,IY+100)
      K=KS
      A = AS
      X = XS
      Y = YS
      Q = QA(K)
      IF(AS.GT.0.) GO TO 10
      YLIM = YA(K)
      GO TO 20
   10 YLIM = YA(K-1)
   20 DELX = DX
   30 B = A+DELX*Q*6080.
      IF (A.EQ.0.) GO TO 115
      IF(SIGN(1.,B).NE.SIGN(1.,A)) GO TO 40
      DELY = 3040.*(B+A)*DELX
      GO TO 50
   40 B = 0.
      DELX = -A/Q/6080.
      DELY = 3040.*A*DELX
      IF(A.GT.0.) GO TO 42
```

```
 1  IF(Y+DELY.LT.YLIM) GO TO 52
    GO TO 70
 2  IF(Y+DELY.GT.YLIM) GO TO 102
    GO TO 70
 0  IF(A.GT.0.) GO TO 100
    IF(Y+DELY.GE.YLIM) GO TO 70
 2  SGN = -1.
    DELY = YLIM-Y
    IF(K.EQ.NMAX) GO TO 60
    K=K+1
    YLIM = YA(K)
 0  B=SGN*SQRT (ABS(A**2+2.*G*DELY))
    DELX = (B-A)/G/6080.
    G = GA(K)
 0  X = X+DELX
    Y = Y+DELY
    IF(X.GE.800.) GO TO 110
    IF(Y.GE.500.) GO TO 120
    IF(Y.LE.0.) GO TO 90
    A = B
 0  IX=X
    IY=Y
    CALL DRWABS(IX+150,IY+100)
    GO TO 20
 0  A = -B
    YLIM = YA(NMAX-1)
    GO TO 80
 0  IF(Y+DELY.LE.YLIM) GO TO 70
 2  SGN = 1.
    DELY = YLIM-Y
    K=K-1
    YLIM=YA(K-1)
    GO TO 60
10  IF(X.EQ.800.) GO TO 120
    X = X-DELX
    Y = Y-DELY
    DELX = 800.-X
    GO TO 30
15  DELY = 3040.*(B+A)*DELX
    IF(G.LT.0.) GO TO 117
    YLIM=YA(K-1)
    GO TO 42
17  YLIM=YA(K)
    GO TO 41
20  IX=X
    IY=Y
    CALL DRWABS(IX+150,IY+100)
    RETURN
    END
```

APPENDIX B

COMPUTER PROGRAM IMAGE

This appendix describes a FORTRAN computer program that calculates and displays optical image distortions created by arbitrary but piecewise linear temperature-versus-height profiles.

Program IMAGE is a FORTRAN IV program designed for use on the Data General Nova 800 minicomputer system using the operating system RDOS. Both input and output of the program is via a Tektronix 4012 interactive graphics display terminal. The purpose of the program is to calculate and display the optical image that an object would exhibit to an observer at an arbitrary range and height above the earth's surface for arbitrary but piecewise linear temperature-versus-height profiles of up to four linear segments. A fixed object corresponding to a free-form ship's profile 20 metres high and approximately 108 metres long is used in the program. Provisions are made in the program for changes in the refractivity based on the optical wavelength of concern. The image is calculated by tracing a series of rays through the atmosphere for uniformly varying elevation angles at the observation point. The one metre high horizontal "slice" of the object's form closest to the height computed by the ray trace at the observation range is then plotted at the apparent height based on the elevation angle at the observation point assuming no refraction.

Figures B-1 and B-2 are sample outputs from program IMAGE. Figure B-1 is for no change of temperature with height and shows an image that corresponds exactly with the object. Figure B-2 is for no increase of temperature up to 26 metres, then a rapid increase over the next 4 metres, and no increase above that point. The image in this case is the undistorted object below and an inverted and slightly extended object at higher elevation angles created by the "trapping" or bending downward effect of the rapid temperature increase in the

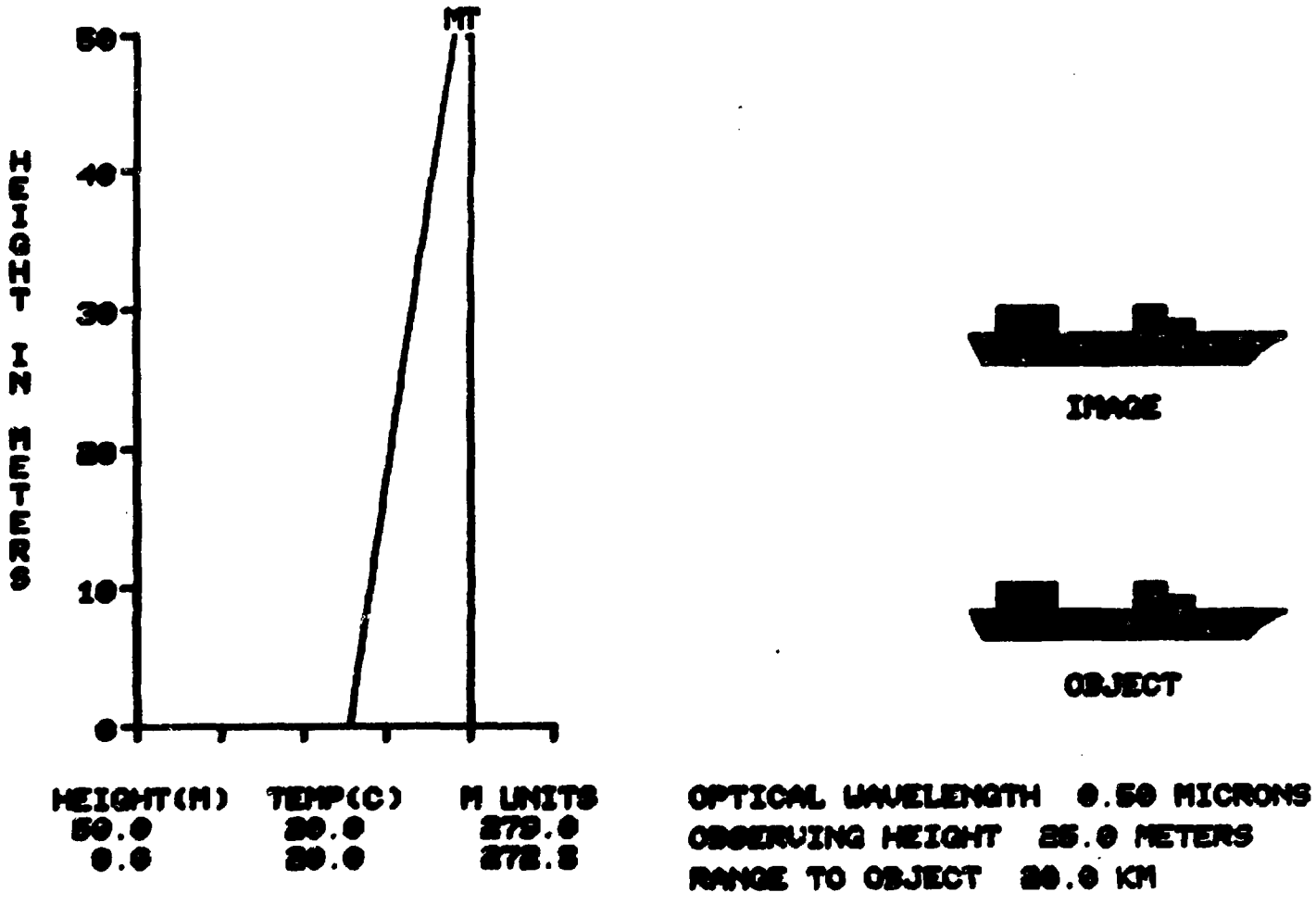

Figure B-1. Image Program Output for the Case of an Isothermal Atmosphere.

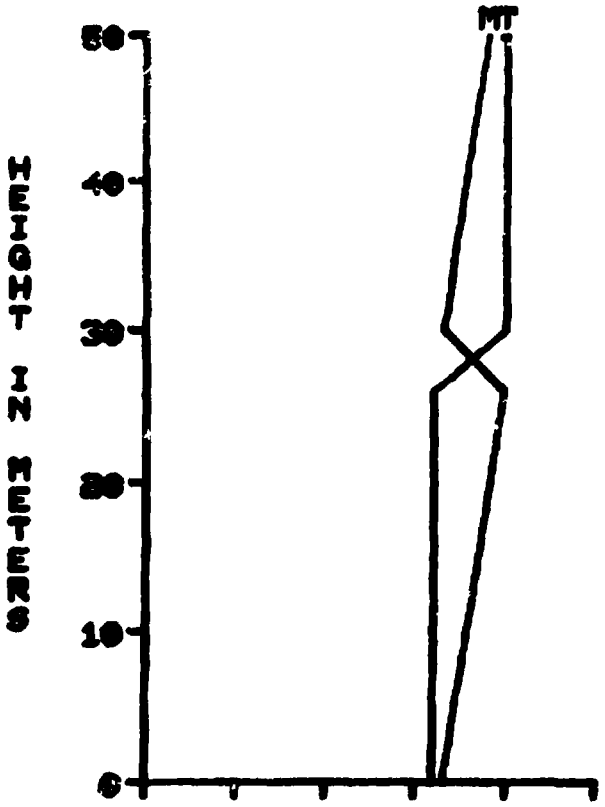

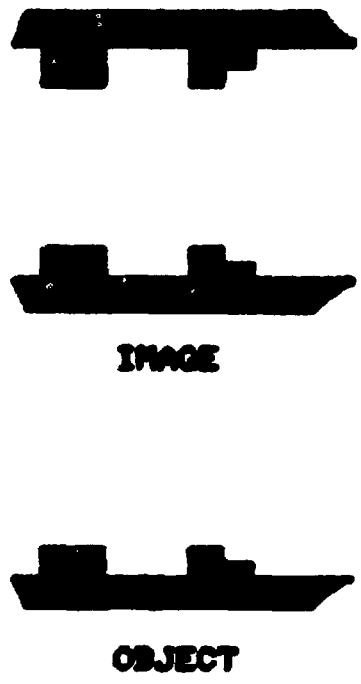

HEIGHT(M)	TEMP(C)	M UNITS
50.0	20.0	279.0
30.0	20.0	278.5
26.0	16.0	279.8
0.0	16.0	276.6

OPTICAL WAVELENGTH 0.50 MICRONS
OBSERVING HEIGHT 25.0 METERS
RANGE TO OBJECT 20.0 KM

Figure B-2. Image Program Output for the Case of a Strong Temperature Increase from 26 to 30 metres.

26 to 30 metre interval. In both cases an optical wavelength of .50 microns, an observing height of 25 metres, and a range to the object of 20 km are assumed. Both temperature in degrees celsius and modified refractivity in M-units are plotted and numerically listed versus height on the output display. Figures B-3 and B-4 are ray trace diagrams that show the trajectories in space of the rays that create the images in Figures B-1 and B-2 respectively.

Figure B-5 is a sample input session for the inputs corresponding to Figure B-2. First the program prompts "ENTER HEIGHT (M), TEMP (C), DESCENDING TO ZERO-5 LEVELS MAX" after which the operator enters up to 5 sets of heights and temperatures. The last height level must be zero. Next, the program prompts "OPTICAL WAVELENGTH (MICRONS) = ", "OBSERVING HEIGHT (M) = ", and "RANGE TO OBJECT (KM) = " after which the operator inputs the required numeric values. This concludes the input session and the program begins calculations.

The program calculates the optical refractivity N from the relation given in reference 1:

$$N = \frac{77.6\ P}{T} + \frac{0.584\ P}{T\lambda^2}$$

where P is atmospheric pressure in mb, T is temperature in Kelvins, and λ is the optical wavelength in microns. The program assumes P decreases with height at a rate of .12 mb per metre starting with a value of 1000 at height zero. The modified refractivity M, which accounts for earth curvature is calculated according to the relation

$$M = N + 0.157\ H$$

where H is height in metres.

The ray trace equations used in program IMAGE utilize small angle approximations since the angles of concern are generally less than 1 to 2 degrees. The

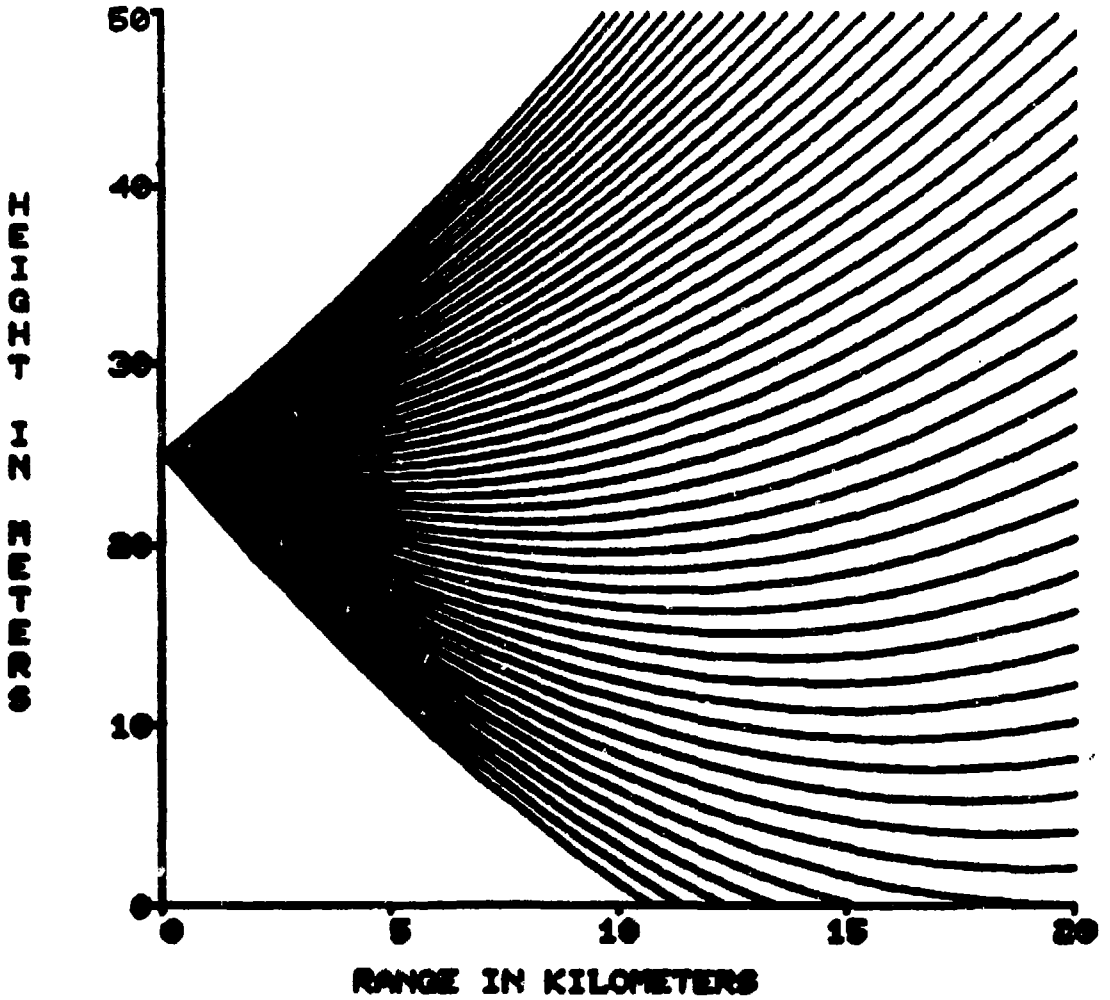

Figure B-3. Ray Trace Diagram Showing the Ray Trajectories for the Image Output of Figure B-1.

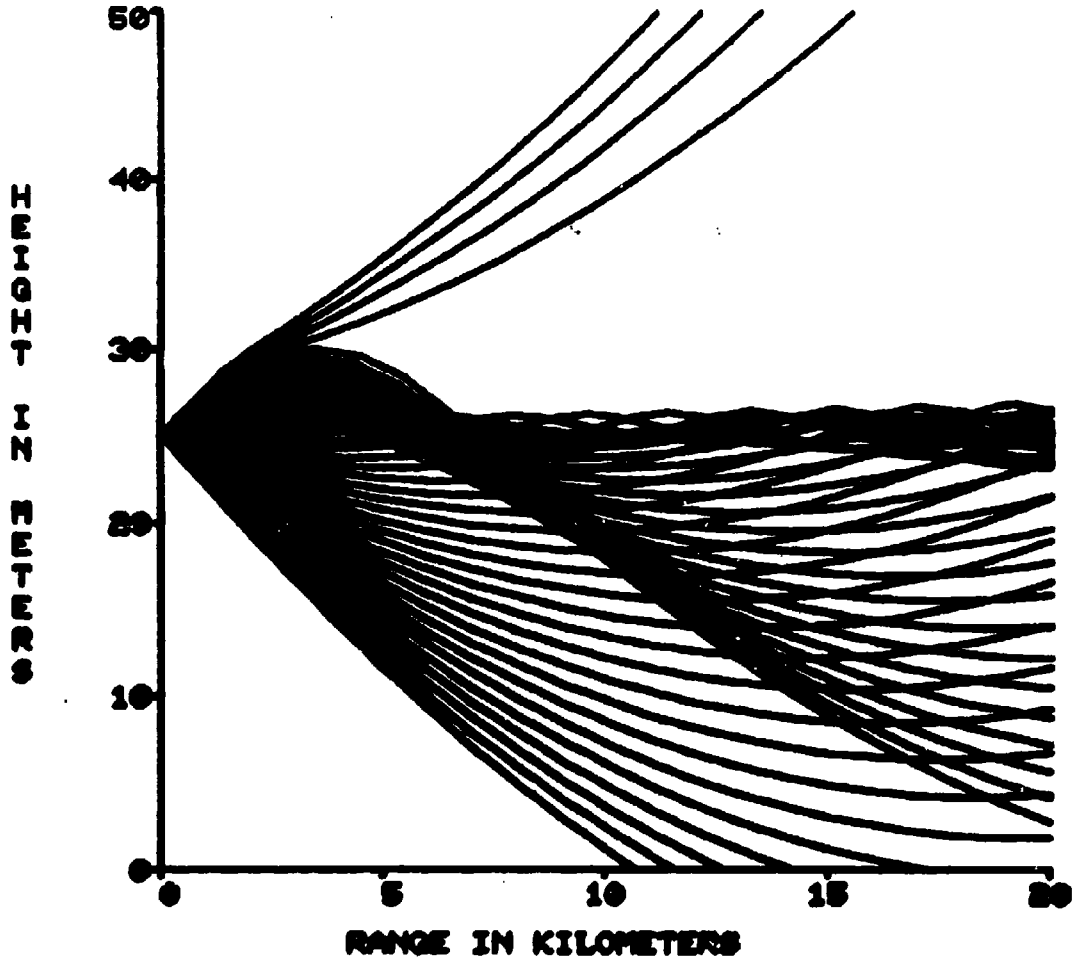

Figure B-4. Ray Trace Diagram Showing the Ray Trajectories for the Image Output of Figure B-2.

```
ENTER HEIGHT (M), TEMP(C), DESCENDING TO ZERO--5 LEVELS MAX
?50,20
?30,20
?25,15
?0,15
OPTICAL WAVELENGTH (MICRONS) ? .5
OBSERVING HEIGHT (M) ? 25
RANGE TO OBJECT (KM) ? 20
```

Figure B-5. Sample Input Session for the Output Shown in Figure B-2.

most important program variables, which correspond to the program listing included in this appendix after the figures, are defined below:

H (I): Height in metres descending with increasing I

T (I): Temperature in degrees celsius corresponding to H (I)

RM (I): M values corresponding to H (I)

RS (I): Gradient $x10^6$ of height to M value for the linear segment below H (I)

$$RS\ (I) = 10^6 \frac{H\ (I) - H\ (I + 1)}{RM\ (I) - RM\ (I+1)}$$

IMAX: Total number of levels. Note H (IMAX) = 0

W: Optical wavelength in microns

HO: Observing height in metres

RKM: Range to object in km

R: Range to object in metres

AS: Elevation angle at observing point for each ray in radians

DELA: Incremental value of AS between successive rays

AO: Elevation angle at beginning of each step along ray in radians

A1: Elevation angle at end of each step along ray in radians

RTOT: Range along ray in metres

RMO: M value at HO

DR: Range increment in metres

HØ: Final value of height in ray increment in metres

The ray trace equations that are used in calculating DR for the various values of H (I) or the final value of height HØ at the observing range are given along with illustrations in Figure B-6. The overall algorithm that increments AS and computes the ray trajectories is best described by the program listing itself.

Reference

1. Thompson, William I., III, "Atmospheric Transmission Handbook," Transportation Systems Center DOT-TSC-NASA-71-6, February 1971.

Case I: Ray penetrating linear region (upgoing or downgoing).

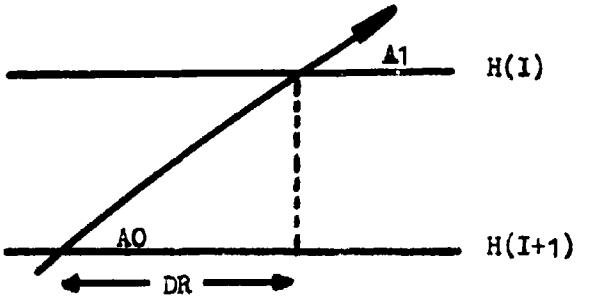

$$A1 = \left[AO^2 + 2 \times 10^{-6} (RM(I) - RM(I+1)) \right]^{\frac{1}{2}}$$

$$DR = (A1 - AO) \cdot RS(I)$$

Case II: Ray maximizing (or minimizing) within linear region.

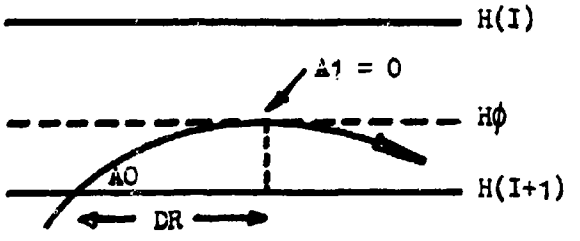

$$A1 = 0$$

$$H\phi = H(I+1) - AO^2 \cdot RS(I)/2$$

$$DR = -AO \cdot RS(I)$$

Case III: Known DR but unknown Hϕ (upgoing or downgoing).

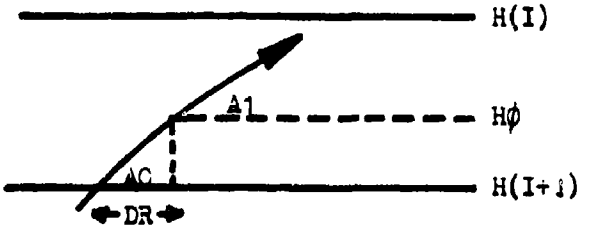

$$A1 = AO + DR/RS(I)$$

$$H\phi = H(I+1) + RS(I) \cdot (A1^2 - AO^2)/2$$

Figure B-6. Formulas and Illustrations for the Three Cases that Need to be Considered in Calculating a Ray Trajectory.

```
C       PROGRAM IMAGE
        COMMON/DUM/ ISHIP(4,20),LABEL(16)
        DIMENSION H(5),T(5),RM(5),RS(5)
        DATA ISHIP/10,100,100,200,9,100,100,202,8,100,100,204,7,100,
       $100,206,6,100,100,208,5,100,100,211,4,100,100,214,3,100,100,217,
       $2,100,100,221,1,100,100,226,20,60,120,160,20,60,120,160,
       $20,60,120,160,20,60,120,160,20,60,120,160,20,60,120,140,
       $20,60,120,140,20,60,120,140,20,60,120,140,20,60,120,140/
        DATA LABEL/'H','E','I','G','H','T',' ','I','N',' ',
       $'M','E','T','E','R','S'/
        CALL INITT(480)
    5 TYPE 'ENTER HEIGHT (M), TEMP(C), DESCENDING TO ZERO--5 LEVELS MAX'
        DO 10 I=1,5
        ACCEPT '=',H(I),T(I)
      IF(H(I).LT.-.001) GO TO 20
   10 CONTINUE
      CALL NEWPAGE
      GO TO 5
   20 IMAX=I
   25  ACCEPT 'OPTICAL WAVELENGTH (MICRONS) = ',W
       ACCEPT 'OBSERVING HEIGHT (M) = ',HO
      ACCEPT 'RANGE TO OBJECT (KM) = ',RKM
      R=1.E3*RKM
      DO 30 I=1,IMAX
       P=1000.-.12*H(I)
      TK=273.+T(I)
   30 RM(I)=77.6*P/TK+.584*P/(TK*W**2)+.157*H(I)
      AS=-2*HO/P
      DELA = 0.5/R
       IMAX1=IMAX-1
       DO 40 I=1,IMAX1
   40 RS(I)=1.E+6*(H(I)-H(I+1))/(RM(I)-RM(I+1))
       DO 50 I=1,IMAX1
       IF(HO.GT.H(I+1)) GO TO 60
   50 CONTINUE
   60 RMO=RM(I+1)+1.E+6*(HO-H(I+1))/RS(I)
      IO=I
       CALL NEWPAGE
      CALL MOVABS(90,200)
      CALL MOVABS(90,200)
      CALL DRWABS(100,200)
      DO 300 I=1,5
      CALL DRWREL(0,100)
      CALL DRWREL(-10,0)
  300 CALL DRWREL(10,0)
      CALL MOVABS(100,190)
      CALL DRWABS(100,200)
      DO 310 I=1,5
      CALL DRWREL(60,0)
      CALL DRWREL(0,-10)
  310 CALL DRWREL(0,10)
      IHMAX=25
      IF(H(1).GT.25.) IHMAX=50
      IF(H(1).GT.50.) IHMAX=100
      YFACT=500./IHMAX
      DO 312 I=1,6
      IH=(I-1)*IHMAX/5
      CALL MOVABS(45,190+(I-1)*100)
      CALL ANMODE
  312 WRITE(10,314) IH
  314 FORMAT(1X,I3)
      DO 316 I=1,16
      CALL MOVABS(10,620-20*I)
      CALL ANMODE
  316 WRITE(10,318) LABEL(I)
  318 FORMAT(1X,A1)
      RMMIN=260.
      RMMAX=285.
      XFACT=300./(RMMAX-RMMIN)
      IX=100+(RM(1)-RMMIN)*XFACT+.5
      IY=200+H(1)*YFACT+.5
```

```
      CALL MOVABS(IX,IY)
      CALL MOVREL(-5,5)
      CALL ANMODE
      TYPE 'M'
      CALL MOVABS(IX,IY)
      DO 320 I=2,IMAX
      IX=100+(RM(I)-RMMIN)*XFACT+.5
      IY=200+H(I)*YFACT+.5
  320 CALL DRWABS(IX,IY)
      IX=100+T(1)*12+.5
      IY=200+H(1)*YFACT+.5
      CALL MOVABS(IX-5,IY+5)
      CALL ANMODE
      TYPE 'T'
      CALL MOVABS(IX,IY)
      DO 322 I=1,IMAX
      IX=100+T(I)*12+.5
      IY=200+H(I)*YFACT+.5
  322 CALL DRWABS(IX,IY)
      CALL MOVABS(0,140)
      CALL ANMODE
      TYPE '     HEIGHT(M)  TEMP(C)   M UNITS'
      DO 330 I=1,IMAX
  330 WRITE(10,340) H(I),T(I),RM(I)
  340 FORMAT(5X,F4.1,6X,F5.1,6X,F5.1)
      CALL MOVABS(500,140)
      CALL ANMODE
      WRITE(10,342) W
  342 FORMAT(' OPTICAL WAVELENGTH ',F5.2,' MICRONS')
      CALL MOVABS(500,110)
      CALL ANMODE
      WRITE(10,344) HO
  344 FORMAT(' OBSERVING HEIGHT ',F5.1,' METERS')
      CALL MOVABS(500,80)
      CALL ANMODE
      WRITE(10,346) RKM
  346 FORMAT(' RANGE TO OBJECT ',F5.1,' KM')
      CALL MOVABS(770,220)
      CALL ANMODE
      TYPE 'OBJECT'
      IXR=700
      IYR=260
      DO 350 IS=1,20
      IH=2*IS
       CALL MOVABS(IXR+ISHIP(1,IS),IYR+IH)
       CALL DRWABS(IXR+ISHIP(2,IS),IYR+IH)
       CALL MOVABS(IXR+ISHIP(3,IS),IYR+IH)
  350  CALL DRWABS(IXR+ISHIP(4,IS),IYR+IH)
      CALL MOVABS(770,420)
      CALL ANMODE
      TYPE 'IMAGE'
      IYR=460
       IH=0
C      BEGIN RAY TRACE
   70 A0=AS
      RTOT=0.
       I=I0
       H0=H0
       RM0=RM0
   80 IF(A0.LT.0.) GO TO 110
      TEST=A0**2+2.E-6*(RM(I)-RM0)
       IF (TEST.LT.0.) GO TO 90
       A1=SQRT(TEST)
       DR=(A1-A0)*RS(I)
       IF(RTOT+DR.GT.R) GO TO 200
      A0=A1
      H0=H(I)
      RTOT=RTOT+DR
       RM0=RM(I)
      IF(I.EQ.1) GO TO 200
      I=I-1
      GO TO 80
   90 DR=-A0*RS(I)
```

```
      IF(RTOT+DR.GT.R) GO TO 200
      H0=H0-A0**2*RS(I)/2
      RM0=RM0-A0**2/2.E-6
       RTOT=RTOT+DR
      A0=0
  110 TEST = A0**2+2.E-6*(RM(I+1)-RM0)
       IF(TEST.LT.0.) GO TO 120
       A1=-SQRT(TEST)
       DR=(A1-A0)*RS(I)
       IF(RTOT+DR.GT.R) GO TO 200
       RTOT=RTOT+DR
       I=I+1
      IF(I.EQ.IMAX.AND.IH.EQ.0) GO TO 225
       IF(I.EQ.IMAX) GO TO 220
       A0=A1
       H0=H(I)
      RM0=RM(I)
       GO TO 110
  120 DR=-A0*RS(I)
       IF(RTOT+DR.GT.R) GO TO 200
       H0=H0-A0**2*RS(I)/2.
      RM0=RM0-A0**2/2.E-6
      RTOT=RTOT+DR
       A0=0.
       GO TO 80
  200 A1=A0+(R-RTOT)/RS(I)
       DM=(A1**2-A0**2)/2.
       H0=H0+RS(I)*DM
      IF(H0.GT.20.) GO TO 220
       IS=H0+1
       CALL MOVABS(IXR+ISHIP(1,IS),IYR+IH)
       CALL DRWABS(IXR+ISHIP(2,IS),IYR+IH)
       CALL MOVABS(IXR+ISHIP(3,IS),IYR+IH)
       CALL DRWABS(IXR+ISHIP(4,IS),IYR+IH)
  220 IH=IH+1
  225 AS=AS+DELA
       IF(AS.LT.3.E-2) GO TO 70
      CALL TINPUT(ICHAR)
      CALL NEWPAG
      IF(ICHAR.EQ.26) GO TO 25
       GO TO 5
      END
```

APPENDIX C

COMPUTER PROGRAM RAYPROP

This appendix describes a BASIC computer program which determines whether a refracted line of sight path exists between a source and receiver located at arbitrary heights above the sea surface.

It assumes the existance of a constant gradient of index of refraction within the range $\infty > dn/dh > -1/a$ (a = radius of earth = 6378.388 km). The user may either input the gradient of his choice of default to the value for the standard atmosphere.

As shown in Figure C-1, the following outputs are available:

1) Distance to source horizon (km)
2) Dip angle to source horizon (mrad)
3) Distance to receiver horizon (km)
4) Dip angle to receiver horizon (mrad)
5) Beam pointing and receiving angles for the refracted line of sight path (mrad)
6) Raytrace from source for arbitrary beam pointing angle and divergence
7) Raytrace printout

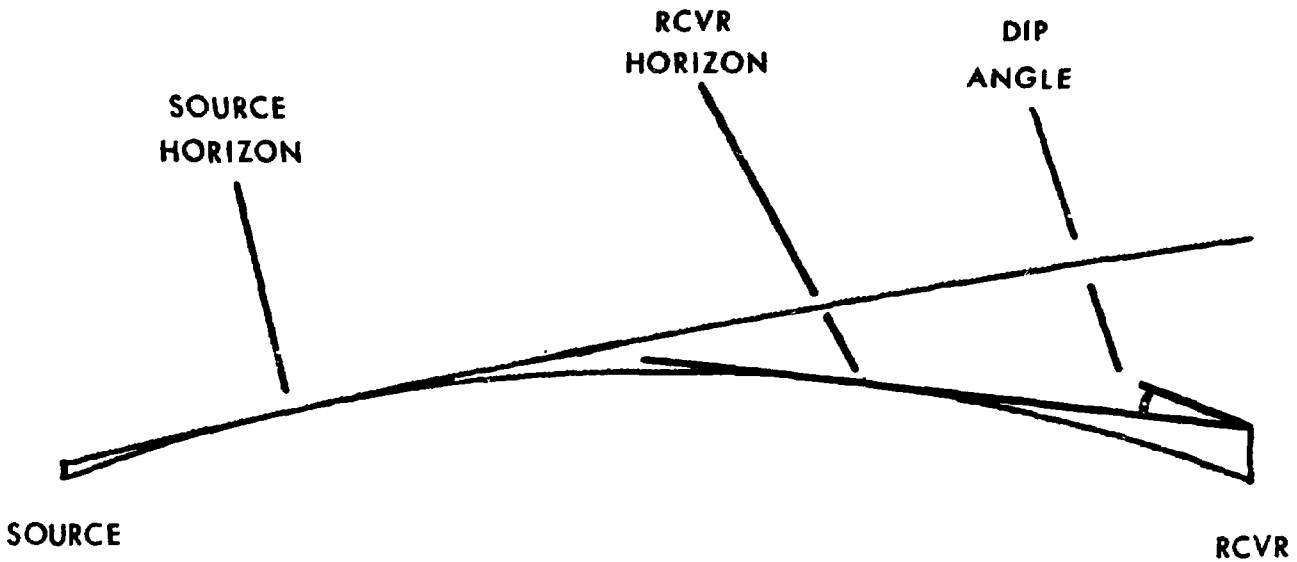

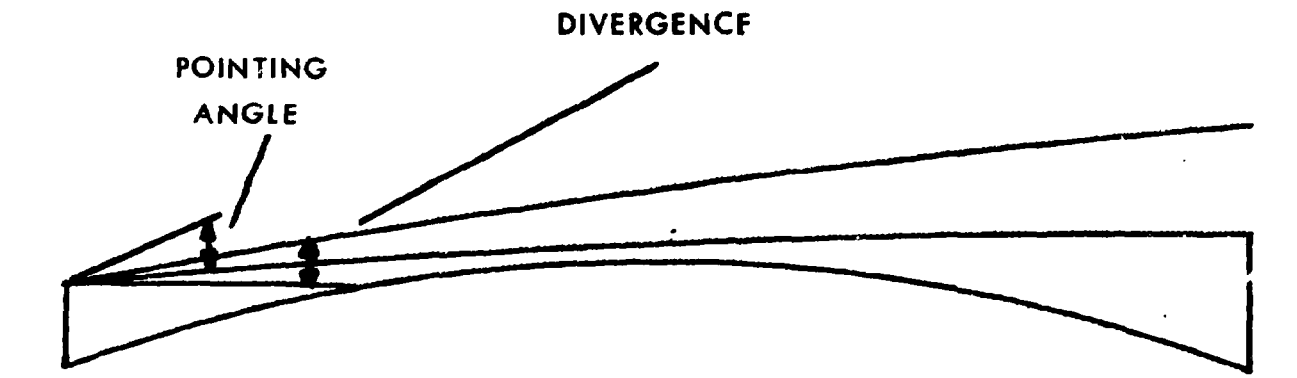

Figure C-1. Sample Outputs and Raytrace for the RAYPROP program.

```
  4 REM     **RAYPROP**
  5 INIT
  6 PAGE
  7 GO TO 100
  8 LET G=-2.3E-8
  9 GO TO 200
 10 GO TO 360
 16 GO TO 998
 20 LET I0=1
 21 IF P>2 THEN 550
 22 GO TO 410
100 REM
102 LET P=0
110 SET KEY
120 PRINT "INPUT SOURCE AND RECEIVER HEIGHTS IN METERS    ";
130 INPUT H0,H1
140 PRINT "_INPUT PATH LENGTH IN KILOMETERS    ";
150 INPUT S
160 PRINT "_INPUT INDEX GRADIENT PER METER OR PRESS"
161 PRINT "USER KEY 2 FOR STANDARD ATMOSPHERE    ";
170 REM     USE NEGATIVE GRADIENTS FOR INDICES
180 REM     WHICH DECREASE WITH HEIGHT.
190 INPUT G
200 LET A=6378.388
210 LET K=1/(1+A*G*1000)
215 IF K>0 THEN 220
216 PRINT "J_"
217 GO TO 320
220 REM     COMPUTE HORIZONS
230 LET Z0=SQR(A*H0*2/500)
240 LET Z1=SQR(A*H1*2/500)
241 LET B0=-H0/Z0-500*Z0/(K*A)
242 LET B1=-H1/Z1-500*Z1/(K*A)
250 PRINT "J_J_J_SOURCE HORIZON = ";Z0;" KM"
251 PRINT "J_SOURCE HORIZON ANGLE = ";B0;" MRADJ_J_J_"
260 PRINT "J_RECEIVER HORIZON = ";Z1;" KM"
261 PRINT "J_RECEIVER HORIZON ANGLE = ";B1;" MRADJ_J_J_"
270 REM     TEST FOR REFRACTED LINE OF SIGHT
280 IF Z0+Z1>S THEN 310
290 PRINT "NO REFRACTED LINE OF SIGHT PATH EXISTSJ_J_J_"
300 GO TO 340
310 PRINT "REFRACTED LINE OF SIGHT PATH EXISTSJ_"
320 LET E0=(H1-H0)/S-500*S/(K*A)
321 LET B1=(H0-H1)/S-500*S/(K*A)
330 PRINT "BEAM POINTING ANGLE = ";E0;" MRADJ_"
331 PRINT "RECEIVING ANGLE = ";B1;" MRADJ_J_J_"
340 PRINT "PRESS USER KEY 3 FOR A RAYTRACE OR KEY 4 TO ENDJ_J_"
350 WAIT
```

```
363 REM    RAYTRACE ROUTINE
370 PRINT "INPUT BEAM INCLINATION AND DIVERGENCE IN MRAD    ";
380 REM    ANGLES ABOVE HORIZONTAL ARE POSITIVE,BELOW ARE NEGATIVE
390 INPUT B0,D
400 REM    DRAW SEA SURFACE
405 LET I0=32
410 PAGE @I0:
420 REM
430 WINDOW 0,S+2,0,13
440 MOVE @I0:1,0
450 FOR L=0 TO S STEP S/200
460 LET X=L+1
470 LET Y=500*L*(S-L)/A
480 DRAW @I0:X,Y
490 NEXT L
500 REM    DRAW SOURCE AND RECEIVER
513 MOVE @I0:1,0
520 DRAW @I0:1,H0
530 MOVE @I0:1+S,0
540 DRAW @I0:1+S,H1
550 REM    PLOT RAYS
560 FOR B=B0-D/2 TO B0+D/2 STEP D/2
570 MOVE @I0:1,H0
580 FOR L=0 TO S STEP S/200
590 LET H=H0+B*L+500*L^2/(V*A)
591 IF H<0 THEN 635
600 LET X=L+1
610 LET Y=H+500*L*(S-L)/A
611 IF Y>10 THEN 635
620 DRAW @I0:X,Y
630 NEXT L
635 IF D=0 THEN 650
640 NEXT B
650 HOME
655 LET P=P+1
660 PRINT "PRINTOUT-KEY 5"
998 PRINT "G_G_G_G_G_
999 END
```